Project No. 608930

FP7-SMARTCITIES-2013

OPtimising Hybrid Energy grids

for smart citieS

WP3 Monitoring and System Analysis

Deliverable 3.4.2

Validation of Metrics for the Comprehension of real-life data with virtual information

H.Ruf[1], D.Funk[1], D.Stakic[1], K.Ditz[1], E.Neuchel[1], G.Heilscher[1], M.Schroedter-Homscheidt[2], Franziska Schnell[2], F.Meier[3]

[1]Ulm University of Applied Science, [2]DLR, [3]Stadtwerke Ulm/Neu-Ulm Netze GmbH

Version:	1.0
Due Date:	31 Aug 2015
Submission Date:	04 Sep 2015
Lead Coordinator:	HS Ulm

Copyright

@ Copyright 2013-2016 The OrPHEuS Consortium

Consisting of

Coordinator	WIP – Renewable Energies (WIP)	Germany
Participants	Hochschule Ulm (HSU)	Germany
	Stadtwerke Ulm GmbH (SWU)	Germany
	Technische Universität Wien (TUW-EEG)	Austria
	Austrian Institute of Technology (AIT)	Austria
	Deutsches Zentrum für Luft- und Raumfahrt EV (DLR)	Germany
	NEC Europe Ltd. (NEC)	UK
	Lulea Tekniska Universitet (LTU)	Sweden
	Skellefteå Kraft (SKR)	Sweden

This document may not be copied, reproduced, or modified in whole or in part for any purpose without written permission from the OrPHEuS Consortium. In addition to such written permission to copy, reproduce, or modify this document in whole or part, an acknowledgment of the authors of the document and all applicable portions of the copyright notice must be clearly referenced.

All rights reserved.

This document may change without notice.

Deliverable Description

Abstract: The main objective of the deliverable D3.4.2 (Task 3.4 Comprehension of real-life data aggregation with virtual information) the validation of the required metrics and their estimation by remote sensing and meteorological forecasts against in-situ and ground-based measurements as so-called virtual (or indirect) measurements. The influence of the two main drivers, the solar irradiance and the air temperature are studied in detail for different locations. The accuracy of satellite-based irradiance measurements from the MACC-RAD service and the irradiance intraday-forecast from the numerical weather prediction of the European Centre for Medium-Range Weather Forecasts (ECMWF) is validated against ground measurements in Germany provided from the German weather service (DWD). The validation of different satellite irradiance products and the data analysis of irradiance effects on the electric grids with higher shares of photovoltaic systems is performed at the demo site Ulm. The air temperature evaluation based on MERRA (Modern Era Retrospective-Analysis for Research) reanalysis data is performed for both demo sites Ulm and Skellefteå. Additionally the air temperature intraday forecast provided by ECMWF is validated against 36 meteorological stations in Germany.

Key Words: ICT, smart cities, hybrid energy grid, energy saving, demonstrations, smart grid, energy control, monitoring, remote sensing, energy meteorology

Document History

Version	Date	Authors	Description
0.1	2015-06-16	HS Ulm	D3.4.2 Draft of deliverable outlining
0.2	2015-08-13	DLR	Review
0.3	2015-08-21	HS Ulm	Changes according review
0.4	2015-08-24	HS Ulm	Final version
1.0	2015-08-25	WIP	Final revision

Dissemination Level

Dissemination Level		
PU	Public	**X**
PP	Restricted to other programme participants (including the Commission Services)	
RE	Restricted to a group specified by the Consortium (including the Commission Services)	
CO	Confidential, only for members of the consortium (including the Commission Services)	

Executive Summary

The OrPHEuS project elaborates a Hybrid Energy Network Control System for Smart Cities implementing novel cooperative local grid and inter-grid control strategies for the optimal interactions between multiple energy grids. This is done by enabling simultaneous optimization for individual response requirements, energy efficiencies and energy savings as well as coupled operational, economic and social impacts. Starting from existing system setups in two European cities (Ulm, Germany, and Skelleftea, Sweden), enhanced operational scenarios are demonstrated for today’s market setup, as well as for future market visions.

The rising rate of volatile energy sources like solar and wind affects more and more the general generation, demand patters and energy grid operation. An efficient operation strategy needs detailed information at the grid level. This required information can be collected by direct measurements at the point of interest, by using indirect measurements of ambient parameters and by simulations with models. The latter two options are denoted as virtual measurements. The application of observation data from remote sensing systems and meteorological forecasts can reduce the costs for the measurement of physical parameters. Therefore, an observation of the hybrid energy grids in high spatial and time resolution can be achieved without further in-situ measurements. However, it is necessary to develop the methodologies to derive the virtual measurements out of various inputs and to validate the virtual measurements against smart meters and transformer voltage. The additional information about the grid state and the forecasts helps to optimize the existing and future control strategies in the different energy grids.

The main objective of the deliverable D3.4.2 (Task 3.4 Comprehension of real-life data aggregation with virtual information) is to validate the required metrics and their estimation by remote sensing and meteorological forecasts against in-situ and ground-based measurements.

First, an overview of the state-of-the-art data sources in energy grids is given. Then two main drivers influencing the different energy grids and being not measured in sufficient detail in nowadays operations, the solar irradiation and the air temperature, are studied in detail for the different energy grids. The different sources for remotely sensed and forecasted information are evaluated. The accuracy of satellite-based irradiance measurements from the MACC-RAD service and the irradiance intraday-forecast from the numerical weather prediction of the European Centre for Medium-Range Weather Forecasts (ECMWF) is validated against ground measurements in Germany provided from the German weather service (DWD), see chapter 3.2. The data analysis of irradiance effects on the electric grids with higher shares of photovoltaic systems is performed at the demo site Ulm (see chapter 3.3 to 3.6). Besides evaluating the meteorological parameters itself, their usage in transformer voltage’s calculation is evaluated via transformer measurements and smart meters. The air temperature evaluation based on MERRA (Modern Era Retrospective-Analysis for Research) reanalysis data is performed for both demo sites Ulm and Skellefteå (see chapter4). Additionally, the air temperature intraday forecast provided by ECMWF is validated against 35 meteorological stations in Germany.

The validation results are adaptable for different climatic areas in Europe and the application potentials for other hybrid energy grid systems across Europe.

Overall, this deliverable contributes to the Scientific and Technical Objective (STO) No. 2 "Adaptation of the existing monitoring systems for the fine-granulated energy network control operations" and therein especially to the 'Comprehension of real-life data aggregation with virtual information'.

The objective of Task 4.2 is the evaluation of control strategies in a simulation environment. Therefore, several input parameters are necessary. In Task 3.4 a validation of several satellite measurements against ground measurements is done for the air temperature and irradiance on tilted planes for specific time-series and locations. These aggregated data are delivered as input parameter for the Task 4.2.

For the task 5.1 the output of D3.4.2 provides an overview of the available data and calculation models. This input is needed for a grid state estimation with the use of virtual data and is necessary for the control strategies within a hybrid grid.

To evaluate the control strategies in a simulation environment there is a need to close the information gaps in the electric grid with high shares of PV. This is done by further direct and indirect measurements and the results are provided to Task 5.3.

A further point is the input of measured and calculated data for the visualization tool, which is subject of the Task 5.4.

Administrative Overview

Task Description

Information about the grid states is essential for control decisions. A result of this directive is the need for metrics to combine data from different sources in simulation and control decision systems. Such data, e.g. electrical power or voltage, can be measured directly and monitored at each important grid point or investigated indirectly by using measurements of ambient parameters e.g. solar irradiance and air temperature in combination with numerical models. The accuracy of the combination of monitoring and simulation will be investigated and compared with the requirements.

In this task the technical solutions for measuring the relevant physical values in the different grid systems will be investigated. Important points are:

- Definition of important grid nodes for monitoring systems
- Evaluation of technical solution for measurement
- Metrics for essential data measurement volume and accuracy for real-life monitoring
- Metrics for essential data point simulations for comprehending real-life monitoring

Relation to the Scientific and Technological Objectives

The task 3.4 is related to the STO2 - Adaptation of the existing monitoring systems for the fine-granulated energy network control operations.

The identified deficit is the high cost for investing and installing in-situ electrical measurements in the distribution grids and the great amount of data which has to be aggregated, filtered and transmitted. Considerations for cost efficiency in system deployment as well as in device selection are mainly driven and solved by quantitative terms within a given cost structure. Comprehension of existing in-situ observations with other means like high-accuracy simulations is lacking.

The general approach in this task is reaching cost efficiency through combination of measurements and simulated values. High-accuracy simulations are performed in order to conclude the definition of critical grid nodes in hybrid energy grids which shall measure directly at the point of interest and which shall be comprehended by accompanied remotely sensed and calculated measurements through system modeling and simulation.

This deliverable defines metrics for the comprehension of in-situ data by using and transforming related information into the parameters being of interest.

Relations to Activities in the Project

The results of the comprehension of in-situ data with the concept of related information is given as input to the simulation (WP4) and control strategy (WP5) work packages. This approach benefits from the analysis of meteorological information (WP3 T3.3).

Partner contribution: The partner HS Ulm extends a pre-OrPHEuS developed numerical model to transform irradiance values in the electric load flow at a distribution transformer and validate the results with measurements at the test site Ulm-Einsingen. Furthermore, HS Ulm extends a standardized transformer oil temperature model. Moreover, HS Ulm analyzes remotely sensed irradiance and temperature data as well as forecast data with several ground stations to determine their accuracy for the application in hybrid energy grids.

The required grid and consumption data and the grid operator oriented application are provided from SWU.

The meteorological data analyses and remotely sensed observation post-processing is provided by DLR.

The OrPHEuS project benefits from the irradiance and air temperature ground measurements of 35 stations in Germany provided from the German weather service.

Terminologies

Abbreviations

BHI	Beam horizontal irradiance
BHI_{cs}	Beam horizontal irradiance under clear-sky conditions
BNI	Beam normal irradiance
BNI_{cs}	Beam normal irradiance under clear-sky conditions
BSRN	Baseline Surface Radiation Network
CC	Correlation Coefficient
DES	Decentralized Renewable Energy Systems
DHI	Diffuse horizontal irradiance
DHI_{cs}	Diffuse horizontal irradiance under clear-sky conditions
DNI	direct irradiation on normal plane
DSO	Distribution System Operator
DWD	Deutscher Wetterdienst (German weather service)
ECMWF	European Centre for Medium-Range Weather Forecasts
GHI	Global horizontal irradiance
GHI_{cs}	Global horizontal irradiance under clear-sky conditions
HC3v4	HelioClim-3
IEA	International Energy Agency
kC	Clear-sky index
MACC	Monitoring Atmospheric Composition and Climate
ME	Mean Error
MERRA	Modern Era Retrospective-Analysis for Research
MS	Milestone
MSG	Meteosat Second Generation
NOSLP	Non-standard load profile based on measurements
OIPT	Oil-immersed power transformers
PV	Photovoltaic
P_{Load}	residuum of the demanded power
P_{MPP}	power at maximum power point
P_{Nom}	Nominal PV module power
P_{PV}	PV feed-in power
P_{Trafo}	load flow at the transformer
PVPMC	Photovoltaic Performance Modelling Collaborative
RMSE	Root Mean Squared Error
SOLEMI	Solar Energy Mining
STO	Scientific & Technological Objective
STD	Standard deviation
SLP	Standard load profile
nME	Normalized Mean Error
nRSME	Normalized Root Mean Squared Error
rME	Relative Mean Error
rRMSE	Relative Root Mean Squared Error

Table of Contents

1. Introduction

The political targets to reduce the CO_2-emission by increasing the energy supply with renewable energies and reducing the demand has led to fast changing situations in the different markets. Nowadays, most of the stakeholders just look on the different energy systems (electricity, district heating and gas) and consider them as separate systems without recognizing the potential synergies of the combination of these different systems into a single hybrid system.

The development of this hybrid system in combination with changing load patterns by local generation and high dynamic in the development of grid technologies leads to a need of more detailed information about the customers, providers and the grids themselves. The consideration of meteorological data and weather predictions becomes more important especially with the volatile characteristic of different renewable sources (wind, solar).

The purpose of this document is to give an overview on the application of remote-sensing and forecast techniques of solar irradiation and air temperature and the usage within the grids. Both influence the demand and generation in hybrid energy grids. Solar irradiation has an impact on the feed-in power of decentralized PV generators and also reduces the demand of heat in buildings by solar gain. The air temperature is main driver of the heat demand and therefore has a strong impact on the gas and district heating consumption. Furthermore, it affects the efficiency of PV systems or heat pumps.

The major objective of this report is the validation of required physical modelling approaches, called 'metrics'. These are determined in order to understand in-situ measurements with the help of observations from remote sensing systems and forecasted values from numerical weather prediction models. This comprehension will lead to a more accurate prediction of the status of the single energy systems.

The priority for measurements is given to the electrical grid because of rare use of storage technologies. The other energy grids have the advantage that storages are available and their usage is state-of-the art or the grid itself has the possibility to be used as storage (e.g. increasing temperature in district heating grids). Furthermore, electric grids show higher dynamic and faster changes in the status.

The in-situ data are measured within the grids and at the connected systems like substations, consumers or generators. These measurements can be improved by using state-of-the-art systems in combination with upcoming technologies. This is the base for an optimized hybrid grid operation. Two grid realisations can be used: Real-time grid operations using measurements of ambient parameters and calculated grid states. Thereby the measured values and accuracy of the system models need to be considered. Moreover, the way from using real-time measurements of meteorological parameters to using forecasted values of the same kind is short and gives the opportunity to forecast the grid's state using the same numerical models. The development of the models and the investigation of the accuracy can be done by historically stored forecast data compared with the measured data at the same location and time. It is expected that the combination of in-situ data, remotely sensed observations, and forecasted values will result in much more accurate data for pro-active grid operations.

Therefore, for the solar irradiation the satellite-based MACC-RAD service is investigated for several locations in Germany. A comparison of MACC-RAD and other commercially available satellite irradiance data is validated against ground measurements in the demo site Ulm, Germany. The application of this irradiance data in grid applications is shown in different stages also for the demo site Ulm. The air temperature of several ground measurements is compared to forecast model data. The data therefore used are reanalysis data for historical periods as well as intra-day forecasts provided from the European Centre of Medium Weather Forecasts (ECMWF).

This report is organized as following:

- Chapter 2 gives a brief overview about the state-of-the-art in the combination of remote sensing technologies and their use in energy-related applications.
- Chapter 3 describes the influence of solar radiation on the demand and generation in the energy grids in combination with an outlook to required data for the areas of interest.
- Chapter 4 discusses the air temperature as parameter for the demand which is satisfied by the various energy systems.
- Chapter 5 concludes the results and give an outlook on further research and development.

2 State-of-the-Art

According to the increasing amount of volatile energy sources there is a need of monitoring systems spatially resolved for all energy grids and on every single power level. Nowadays, the different energy grids have a lack of information. Therefore, additional information is needed to achieve the goal of a corporate control strategy for the hybridisation of the energy grids. The monitoring system is well developed in the higher power level like for example in the electric grid. There is a real-time monitoring of the transmission station and lines installed in the high voltage grid. When going to the lower power levels the monitoring level is decreasing. In the low voltage grid only the annual consumption and the peak power flow over the transformer are measured. Furthermore the monitoring in the gas and the district heating grid has also no complete observation.

Depending on national law the distribution grid operators (DSOs) are able to collect data from large decentralized renewable energy systems (DES) at the grid connection point from specialized feed-in management devices. Furthermore, several states in the European Union have started with the roll-out of smart meters while others are still in the regulation process [1], [2]. Smart meters providing time-series of energy instead of an annual sum and can deliver the necessary data to describe the state of the grid [3] and a secure communication channel to controllable local systems [4]. These are also in-situ measurements but not necessary available for DSOs in real-time. These data could be used as supporting points in grid simulation as well as supporting points for pro-active grid supporting system similar to the synoptically data mining of meteorological weather forecast systems.

Another option to collect data is the monitoring of DES by commercial providers. For example, PV systems often use monitoring devices connected to the inverters in combination with local irradiance measurements or satellite derived irradiances [5]. These data are stored in databases of the providers and used for different services to the customers, but is generally not being forwarded to grid operators without any payment or limited by privacy regulations. So other sources need to be used to get further information about the DES for the grid operation.

A large area benefits from a sufficient number of both PV systems and consumers that allows the usage of statistical equivalent characteristics and lumped PV models, representing the average response of the PV fleet. In areas of smaller size such as the low voltage grid served by a single transformer station the behavior based on statistical analyses cannot be assumed. Therefore, more detailed information and accurate calculations of the P_{PV} of the single PV systems are required.

To increase the information of the low-voltage grid with high shares of residential PV systems irradiation can be taken out of satellite measurements to calculate the actual power of the PV systems. This approach avoids the measurement equipment cost of around 3,000 € at the transformers. These costs are only for the measurement hardware and neither considers the installation and connection to the control centre nor the operational costs. In Germany, there are at least 560,000 transformers installed and hardware installations can reach costs of several million Euros. The common irradiation models focused on hourly data can also be used with much finer time resolution of 1-minute. Depending on the quality of the data source the every minute bias error is equal to the hourly bias error. The use of input data of lower quality decreases the performance of the transposition models significantly. Therefore, the main factor is the separation of the direct and diffuse irradiation [6]. The calculation of the PV feed-in power (P_{PV}) based on the irradiance can be realized by highly accurate models for single PV systems or by statistical models for lumped PV fleets. The decision which model has to be used depends on the required accuracy and available input parameters.

Such approaches exist in the electric system in high power level [7] and are under development for low voltage grids [8]. Furthermore, it is expected that such approaches are adoptable to other energy grids e.g. district heating or gas grids. The investigation topics will be different and the models have to be developed. Further input parameters like the air temperature or wind speed will also be necessary.

The generation of volatile DES and the demand patterns depend on the weather conditions. Control strategies can be profit from the expected information in advance. The main meteorological parameters affecting the energy within hybrid grids in cities are the solar irradiation and the air temperature. These parameters can be forecasted using meteorological forecast techniques. The state of the art of solar and PV forecast is described by the task 14 of the PVPS-program of the International Energy Agency (IEA) [9]. The IEA Task 46 performed a benchmark of existing numerical weather prediction systems for Europe [10].

Furthermore, weather forecasts are used for the prediction of the energy output of volatile generators e.g. photovoltaics (PV) or wind. These forecasts are usable for the monitoring providers as well as for the grid operators. The forecasts are based on remote sensing data from ground stations, planes, satellite data etc. and the prediction are calculated by different numerical algorithms to reach different forecast horizons. Both national and commercial weather service providers consider more and more the demand from the energy sector. The two research sectors “Energy” and “Meteorology” are combined in a new field of research: Energy Meteorology. It is interfacing renewable energy and atmospheric physics by providing data and developing new methods for the characterisation of the fluctuating power output from solar and wind energy systems. For example, as a result of the German research project EWeLiNE [11] the German weather service extended the forecast horizon of the probabilistic numerical weather prediction (COSMO-DE-EPS 03 UTC runs) from 27 hours to 45 hours to fulfil a demand for the day-ahead energy trading. The objective of the EWeLiNE project is a significant improvement of power forecast for renewable energies.

Nowadays the utility and system operators on both transmission and distribution level need the ability to forecast the variable power sources. This need is not limited to the electric system and will become more important with hybrid grids. There are several possible forecasts like e.g. sub-hourly, hour ahead and day ahead and each forecast has advantages for certain tasks in the energy systems.

3 Solar Irradiance

3.1 Overview

Solar irradiance is an important but volatile parameter in the field of renewable energy. The irradiance can be used as source for generating electricity (via photovoltaic systems) or for heating and cooling systems (via solar thermal systems). Furthermore, it affects also the consumption of heat and electric power. This is caused by external yields into buildings or as self-consumption supporting systems.

For these reasons, solar irradiance influences the operation and power transmission and distribution in the different energy domains and has to be investigated and considered in hybrid grid controls. Especially in the distribution grids there is a lack of necessary information to operate grids in a smart and effective way.

Solar irradiance monitoring can be arranged in two ways: ground measurement and calculation from satellite images. Ground based measurements have higher accuracy and temporal resolution of the investigated site. However, the spatial representation is limited and the measured data are valid only for a single location. Ground measurements are operated by meteorological observation networks e.g. BSRN or DWD [12], [13] or by professional monitoring service providers of PV systems.

Satellite derived solar irradiance data are mostly calculated with the Heliosat approach [14] and different improvements [15], [16] using images from geostationary weather satellites (e.g. Meteosat Second Generation). The temporal and spatial resolutions depend on the used algorithms and satellite instruments. State-of-the-art services like the HelioClim databases [17] or the MACC-RAD service provide time series of global (GHI), direct (BHI) and diffuse (DHI) irradiations on horizontal surface, and direct irradiation (DNI) on normal plane for the actual weather conditions as well as for clear-sky conditions. The spatial resolution is 3 x 3 km² at nadir, and approx. 3 x 5 km at 45° of latitude. Data are available with a time step or summation time ranging from 15 min to 1 month.

Based on the requirements, it has to consider if power or energy values are used. *Irradiation* is the energy received per area. It is expressed in Wh/m^2. *Irradiance* is defined as a power received per area. It is expressed in W/m^2.

Based on the benchmarking guidelines of solar radiation products developed during the MESoR project [18], the root-mean-squared error (RMSE), mean error (ME) and correlation coefficient (CC) are important statistical values to describe and compare results, as in equations (1)-(3). These measures are defined by:

$$ME = \frac{1}{N}\sum_{i=1}^{N} x_s(i) - x_m(i) \tag{1}$$

$$RMSE = \sqrt{\frac{1}{N}\sum_{i=1}^{N}\left(x_s(i) - x_m(i)\right)^2} \tag{2}$$

$$CC = \frac{\sum_{i=1}^{N}\left(x_s(i)-\overline{x_s}\right)\cdot\left(x_m(i)-\overline{x_m}\right)}{\sqrt{\sum_{i=1}^{N}\left(x_s(i)-\overline{x_s}\right)^2\cdot\sum_{i=1}^{N}\left(x_m(i)-\overline{x_m}\right)^2}} \quad (3)$$

with N as the total number of measurement data points, $x_s(i)$ as simulated data at time i and $x_m(i)$ as measured data at time i. The relative values of ME and RMSE are rated to the mean values of the measurements.

The corresponding relative measures are related to the mean of the absolute measured values and given by:

$$rME = \frac{ME}{\overline{|x_m|}}\cdot 100\% \quad (4)$$

$$rRMSE = \frac{RMSE}{\overline{|x_m|}}\cdot 100\% \quad (5)$$

Furthermore, to analyze the PV system size independent ME and RMSE are normalized to the rated PV power P_{nom}. These measures are denoted as nME and nRMSE and are given by:

$$nME = \frac{ME}{P_{Nom}} \quad (6)$$

$$nRMSE = \frac{RMSE}{P_{Nom}} \quad (7)$$

3.2 Solar irradiance data from satellites

In future, it will be necessary to know the recent and upcoming P_{PV} of each single installed PV systems. This is caused by the growing number of PV systems connected to the grid. For the calculation of the generated electrical power of a PV system a various number of simulation models are available, e.g. [24] [25]. The irradiance on the PV module plane is necessary to simulate the P_{PV}. The installation of ground based irradiance sensors within the area of interest is one possibility for the DSO to determine the irradiance and calculate the PV feed-in power within a grid area. However, the investments for such monitoring including the installation and maintenance cost are high. Furthermore, these systems only provide point measurement data. Another option is to order a commercial service provider with the calculation of the P_{PV}. Mostly, these providers use private or public measurement networks in combination with remotely sensed data and output of numerical weather predictions.

The irradiance data are derived from Meteosat Second Generation (MSG) satellite images with a procedure based on the Heliosat method. The Heliosat method was originally introduced by Cano et al [14] and further improved, e.g. [15], [39], [40], [41].

Local point measurements of the irradiation can be replaced by satellite-based surface measurements. For example, the pre-operational atmosphere service of Copernicus is currently provided through the FP7 projects MACC and MACC-II (Monitoring Atmospheric Composition and

Climate) [26]. Within the radiation subproject (MACC-RAD) existing historical and daily updated databases for monitoring incoming surface solar irradiance are further developed. The service radiation values at the ground level fulfilling the needs in European and national policy developments and the requirements of partly commercial downstream services, e.g., for planning, monitoring, efficiency improvements, and the integration of solar energy systems into energy supply grids [27].

The MSG satellite data have spatial resolution of 3 x 3 km² at nadir and approximately 5 x 3 km² at the demo site Ulm. The images are provided in 15 minute resolution. The MACC-RAD service with a 15-minute time resolution is based on the new Heliosat-4 approach [20], [19].

Heliosat-4 uses two different irradiance models to realize the decoupling approach mentioned before: McClear and McCloud. McClear is a new irradiance model calculating the down welling solar irradiances under clear-sky conditions using physical relations pre-calculated and stored in look-up tables. This leads to calculation time savings compared to other radiative transfer models. The McCloud model calculates the clear-sky indices for global and beam irradiance under cloudy conditions taking into account cloud properties. Heliosat-4 takes into account various atmospheric input parameters affecting the results [19], [20]. However, the results are usable for a DSO and support the determination of the grid situation. Local deviations are caused by the difference of point and area measurements [28] as well as micro-climatic conditions and have to be considered.

In the following section different Heliosat-method implementations using the data from the same satellite are compared with the ground measurement at the demo site Ulm. The data from MACC-RAD are used to investigate the accuracy at different locations.

3.2.1 Comparison of satellite-derived irradiance data with ground measurements at the city of Ulm

This section describes the comparison of three satellite irradiance data used with ground measurements in the demo site Ulm.

The irradiance data from the Solar Energy Mining (SOLEMI) database are provided by DLR for the location of the weather station at the campus of Ulm University of Applied Science and for the test site. The data set contains hourly average values for GHI, DHI and BNI as well as GHI_{cs}, DHI_{cs} and BNI_{cs} for clear-sky conditions.

MINES ParisTech provided data from the HelioClim-3 (version 4, denoted as HC3v4) database. The data set contains 15-minute average values for GHI, GHI_{cs}, DHI and BHI as well as GNI, DNI and BNI. Both SOLEMI and HC3v4 data are computed with the Heliosat-2 method and differ in the time resolution and the clear-sky irradiance model.

The MACC-RAD service (version 2.6, available under http://www.soda-pro.com) provides public and online irradiance data for dates later than 1st February 2004. The irradiance data are computed with the Heliosat-4 method [19], [20], [21]. The dataset contains 15-minute average values for GHI, DHI, BHI and BNI as well as GHI_{cs}, DHI_{cs}, BHI_{cs} and BNI_{cs} for the locations mentioned above.

For the year 2012, all irradiance data (SOLEMI, HC3v4 and MACC-RAD) are compared with the related 15-minute averages of the ground station at the university campus. The SOLEMI data are linearly interpolated to 15-minute time resolution. The analysis is performed following the guidelines for benchmarking of single point broadband solar radiation data according to [18]. The comparison considers all data pairs with a sun elevation angle above 15° and a ground measured value of at least 10 W/m².

Figure 1 shows the scatter plots of the comparison for all three satellite irradiance services. The main diagonal is shown as the chain dotted line and indicates a perfect measurement without error. All measurements follow and scatter around this main diagonal. The corresponding clear-sky index kC is illustrated with the different colours. The clear-sky index describes the influence of the clouds as a ratio of GHI at ground level related on GHI_{cs} under clear-sky conditions. For clear-sky situations kC is one, for overcast situations kC is zero. Red illustrates high kC values while blue indicates low kC values. The results for the single satellite sources are:

- SOLEMI:
  - ME is 17.08 W/m² (rME 4.49 %)
  - RMSE is 118.41 W/m² (rRMSE 31.10 %)
  - CC is 0.90.
- HC3v4:
  - ME is -18.08 W/m² (rME -4.75 %)
  - RMSE is 101.45 W/m² (rRMSE 26.65 %)
  - CC is 0.92.
- MACC-RAD:
  - ME is 22.98 W/m² (rME 6.04 %)
  - RMSE is 117.69 W/m² (rRMSE 30.91 %)
  - CC is 0.90.

The black solid lines indicate the linear regressions. All values are 15-minute averages.

The highest irradiance with almost 1100 W/m² and the lowest ME are given for SOLEMI. MACC-RAD shows a slightly larger ME, but performs similar to SOLEMI in RMSE, while HC3v4 shows the best RMSE. In terms of CC all datasets are very similar and well correlated. The scatter plot of MACC-RAD shows higher scatter values above the main diagonal axis indicating an overestimation which is also visible in the positive ME.

These results are in the range of other research studies [22], [23]. It can therefore be assumed that there are no local effects in the area of Ulm blocking the usage of the satellite data.

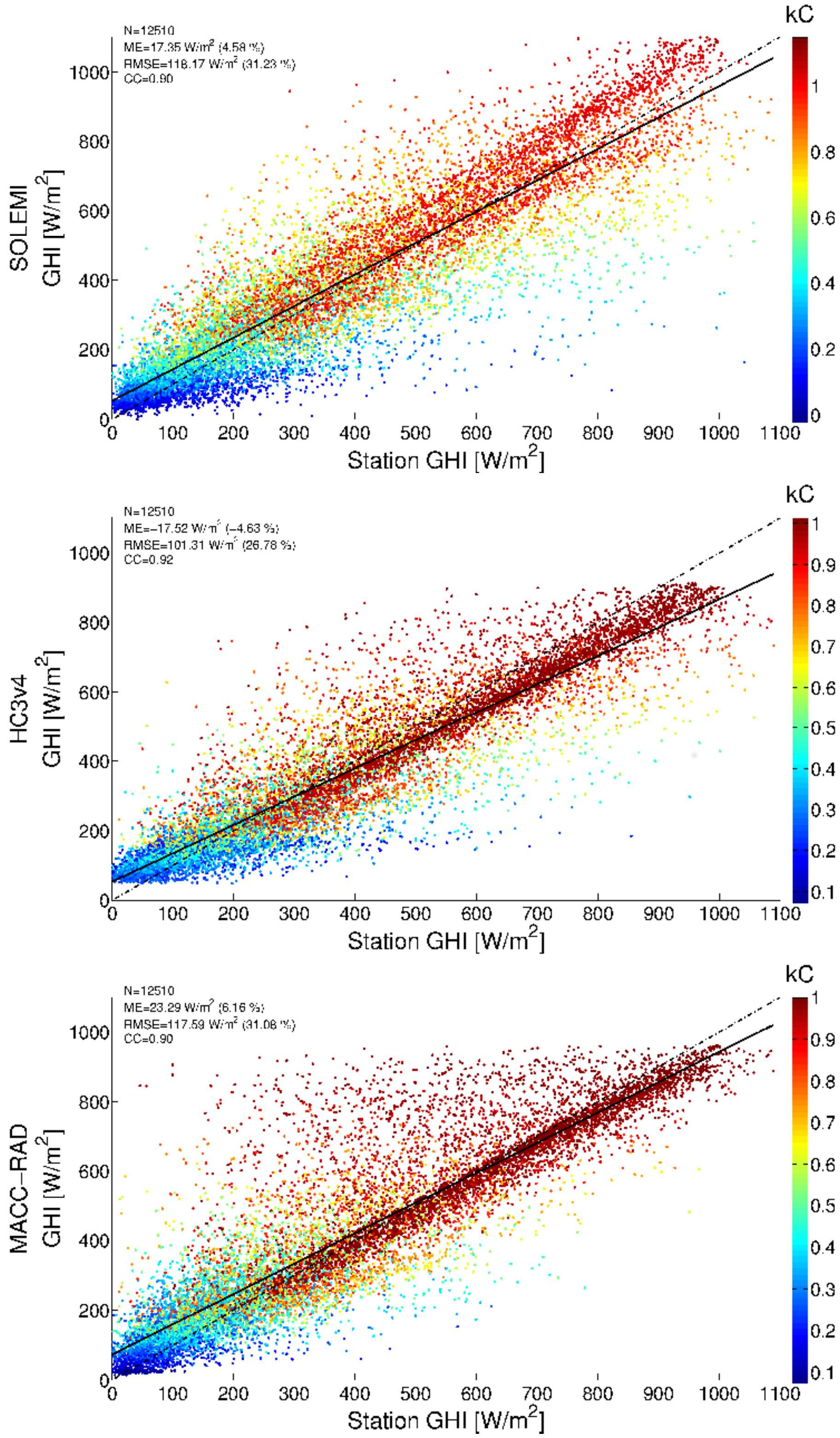

Figure 1: Comparison between ground measured GHI (Station GHI) and satellite measured GHI of SOLEMI, HC3v4 and MACC-RAD for the year 2012.

3.2.2 Comparison of MACC-RAD and ground measurements in Germany

The comparison before is done for a single location and do not represent the accuracy for larger areas. Therefore, a comparison of the MACC-RAD irradiation is done by HSU in cooperation with DWD to determine the accuracy of this dataset. This comparison is based on 35 meteorological ground stations in Germany provided by the DWD and considers the data from the years 2010 to 2013. The data of the DWD measurements are hourly totals and are compared also with hourly data of MACC-RAD. The locations of the different weather stations are shown in Figure 2. The investigated stations are equipped with two different measurement systems. Circles mark stations with Scanning Pyrheliometer/Pyranometer (SCAPP) measurement devices. The SCAPPs measure BHI and DHI and calculate the values of GHI and the sunshine duration within the instrument. The diamonds mark stations equipped with pyranometers measurement devices. Pyranometers measures GHI and can measure DHI if a shadow-band is installed. The BNI measurement requires a so-called pyrheliometer tracking the sun during the diurnal course. Generally, pyranometer and pyrheliometer are used as reference instruments according to WMO because of their high precision. Former studies validate the measurements of SCAPP devices against those of reference instruments and show a slightly higher error of the SCAPP measurement [43]. The altitudes of the weather stations range from 4 m to 2,964 m. The comparison is based on ME, RMSE and CC. The data from the DWD are measured in True Solar Time because of historical reasons and therefore the data has to be transformed into UTC time format by a linear interpolation.

Table 1 gives an overview of the DWD weather stations used. Included are station number used in the result plots, the name of the city, the latitude and the longitude as well as the altitude.

Table 1: Overview about the used weather stations with geographical coordinates and the altitude [13]

#	City	Latitude [°]	Longitude [°]	Altitude [m]
1	Braunlage	51.73	10.60	607
2	Braunschweig	52.29	10.45	81.2
3	Bremen	53.05	8.8	4
4	Chemnitz	50.79	12.87	418
5	Coburg	50.31	10.97	344.5
6	Dresden	51.13	13.76	227
7	Fichtelberg	50.43	12.96	1,213
8	Freiburg	48.02	7.84	236.3
9	Fürstenzell	48.55	13.35	476.4
10	Geisenheim	49.99	7.95	110.2
11	Giessen	50.61	8.65	202.7
12	Görlitz	51.16	14.95	238
13	Halle	51.51	11.95	93
14	Hamburg	53.64	9.99	11
15	Harzgerode	51.65	11.14	404
16	Hohenpreissenberg	47.80	11.01	977
17	Konstanz	47.68	9.19	442.5
18	Leinefelde	51.39	10.30	356
19	Lindenberg	52.21	14.12	98
20	List	55.01	8.41	26
21	Norderney	53.71	7.15	11
22	Nürnberg	49.50	11.06	312
23	Potsdam	52.38	13.06	81
24	Rostock	54.18	12.08	4
25	Saarbrücken	49.21	7.11	320
26	Schleswig	54.53	9.55	43
27	Seehausen	52.89	11.73	21
28	Stuttgart	48.83	9.20	314.3
29	Trier	49.75	6.66	265
30	Weihenstephan	48.40	11.70	477.1
31	Weissenburg	49.02	10.96	422
32	Wittenberg	51.89	12.65	105
33	Würzburg	49.77	9.96	268
34	Zinnwald	50.73	13.75	877
35	Zugspitze	47.42	9.96	2964

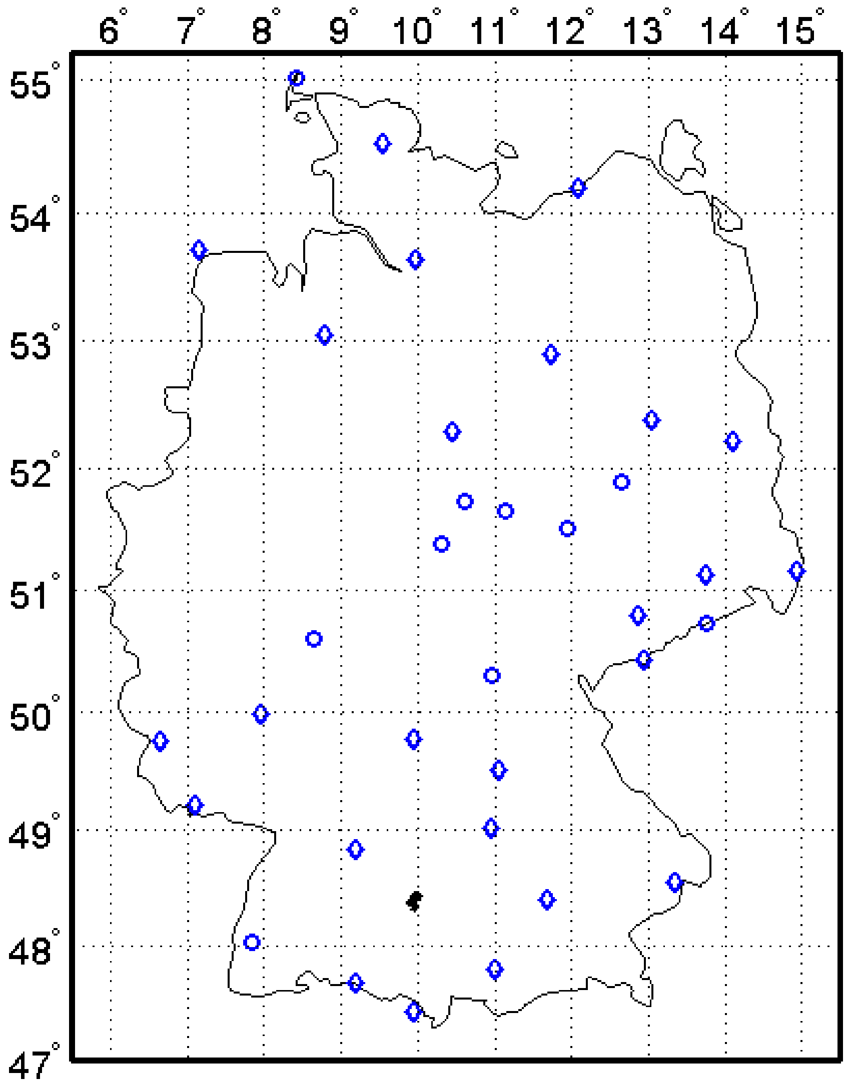

Figure 2: Location of the meteorological stations equipped with irradiance measurements and operated by the DWD. Circles mark stations with SCAPP measurement devices, diamonds mark stations with pyranometers. The small black polygon shows the location of the city of Ulm.

In Figure 3 the values of the ME for GHI measured from the DWD weather station against calculated GHI from the MACC-RAD service are illustrated. The range of the values is from -18 W/m² to 59 W/m². The ME values, except of one location 21 (Norderney), are positive meaning that MACC-RAD overestimates the solar irradiation. Detailed analyses of the single stations are in progress. In Figure 3 complementary the rME is shown with red crosses. The range of the rME of the different locations reclines between -5 % to 18 %. The validation data of the MACC-RAD service takes into account only one weather station in Germany (19, Lindenberg). This station is part of the BSRN network [30]. The rME of the MACC-RAD validation data is 6 % for this location. Up to now, MACC-RAD is validated against 14 BSRN stations, three stations operated by CSP Service and one station operated by DLR all over the world and the rME ranges from 1 % to 13 % [30]. Therefore, the presented results are assumed as plausible.

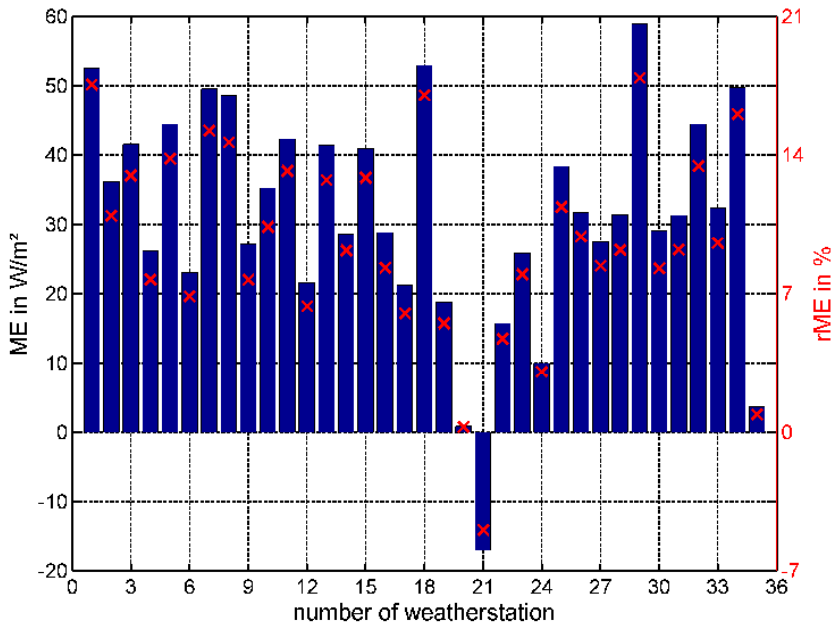

Figure 3: ME (blue bars) and rME (red crosses) of GHI from MACC-RAD compared with for GHI from DWD weather stations for the period of 2010 to 2013.

The RMSE of GHI from MACC-RAD related to GHI measured from DWD weather stations are shown in Figure 4. The RMSE ranges from 75 W/m² to 178 W/m². For the weather station 35 (Zugspitze), a very high RMSE is detected because of the high variability at this location. The reason for this outlier is assumed by the geographical and climatic conditions in high altitude alpine region. Furthermore, the station number 29 (Trier) has a high RMSE. The reason for this outlier is unknown yet, so additional investigations have to be done. The range of the rRMSE (red crosses in Figure 4) is from 22 % to 45 %, with a value of 26 % at Lindenberg location. In comparison, the range for all the validation weather stations of BSRN was from 11 % to 34 %. Therefore, irrespective of the two outliers mentioned before, the investigated data in this work are plausible.

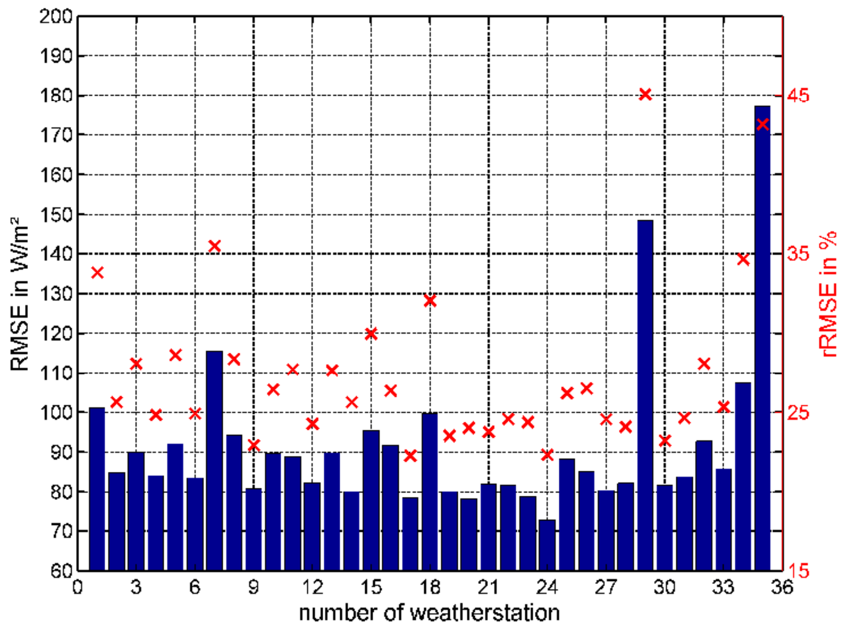

Figure 4: RMSE (blue bars) and rRMSE (red crosses) of GHI from MACC-RAD compared with for GHI from DWD weather stations for the period of 2010 to 2013.

In Figure 5 the CC for the comparison between the measured GHI from the DWD stations against the measured GHI from MACC-RAD are shown. Except two stations, the CC range from 0.91 to 0.96 which means a very good correlation between the ground data and the satellite/model data. The outliers are again the stations 29 (Trier) and 35 (Zugspitze) which are noticeable in RMSE, too. The CC of the validation data set of the MACC-RAD service (station 19, Lindenberg) is 0.95 [30]. The CCs of all validation stations used range from 0.91 to 0.97. Except both outliers the CC of the weather stations in Germany are in line with the validation data of MACC-RAD.

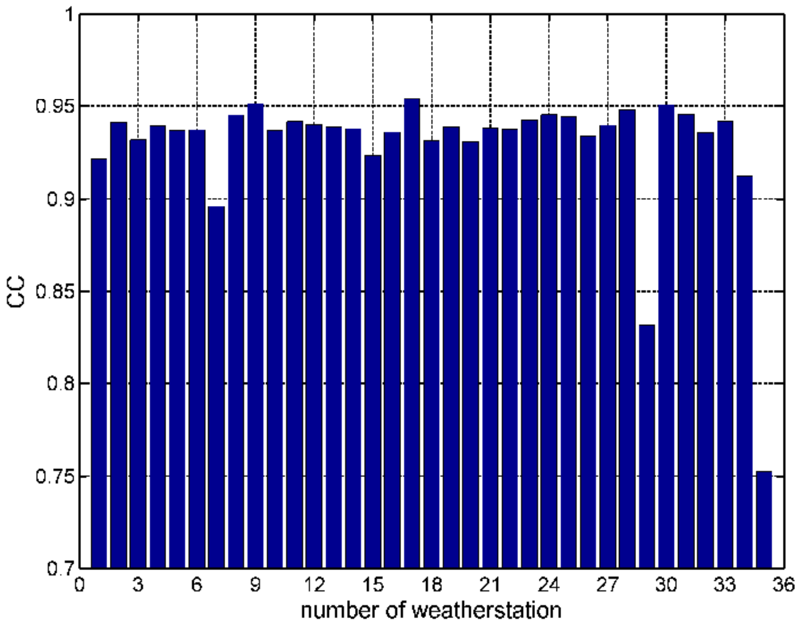

Figure 5: Correlation coefficient for the comparison between GHI from DWD weather stations and calculated with MACC-RAD.

The statistical results of the calculated GHI show the expected deviation to the ground based GHI measurements as given in the validation data.

3.3 Calculation of the Photovoltaic feed-in power in small-scale distribution grid areas

The transformation of solar irradiance into P_{PV} needs a statistical or physical model. The decision which model is required depends on the available data and the needs of the grid operator. Large areas like for transmission system operates with statistical approaches. Small areas like a single transformer or a single PV system provides higher accuracy using a physical model with several parameters. This is studied by modeling PV systems in the area of Ulm test site Einsingen. An example of a model and its application for P_{PV} and transformer power calculation is described and validated in the following section.

3.3.1 Modeling approach

The calculation of the P_{PV} for each PV system is performed with the function toolbox PVLib provided by the Photovoltaic Performance Modelling Collaborative (PVPMC) [25]. This library offers the flexible input of detailed meteorological data in the electrical system modelling of PV systems.

For the irradiance data, required input parameters are information on GHI, DHI and BHI on the horizontal plane delivered by MACC-RAD. From this input and data on the systems latitude and longitude, the irradiance in module plane is calculated, using the approach of Reindl et al. [31], [32] for the diffuse part. As mentioned before, the azimuth angle and tilt angle are taken from [33].

The treatment of the ground reflected part is calculated as given in [34] with a constant albedo value of 0.2. The parameters for those calculations are constant for each system and each time step.

Air temperature and wind speed are delivered by the ground-based meteorological station operated by HS Ulm. The PV system simulation uses the calculated tilted and direct/diffuse split irradiances and the air temperature to calculate the cell temperature reducing the efficiency of the PV array.

For the system modelling a PV model is selected from the PVLib library considering the mostly used cell-technology (poly-crystalline silicium) in Germany and in market since a couple of years. This information refers to the Sandia PV Array Performance Model and Sandia Performance Model for Grid-Connected Photovoltaic Inverters coefficients [35], [36]. The chosen PV module type for the simulated PV system is Yingli Solar YL230-29b together with one Blueplanet 6400xi supreme inverter produced by Kaco New Energy GmbH as the inverter type. This combination was chosen because the market share of crystalline silicon PV systems has always been in the range of 80 to 90% with a slight majority of poly-crystalline silicon technology [37].

The setup of all PV modules and the inverter leads to a PV generator with 28 modules from the type mentioned before, divided into two strings with 14 modules each. Typically, only the nominal power P_{nom} of the PV system and the location of the connection points are known by the DSO. The calculated output power time series of this reference PV system is normalized to the PV generator P_{nom} under standard test conditions (1 kW/m², 25 °C, AM 1.5) Afterwards, the normalized P_{nom} scaled up to the P_{nom} of the installed PV modules at the test site respecting the different PV module orientations of each PV system. In the simulation it is assumed that losses from the system setup (e.g., wiring losses) and from the maximum power point tracker of the inverter are negligible.

The P_{PV} is calculated for each single PV system in 15 minute averages.

3.3.2 Validation with measured feed-in power data

This section describes the validation of satellite-based estimates of P_{PV} versus the smart meter measurements obtained at each PV system.

The investigated test site Einsingen is a suburban neighbourhood in the city of Ulm, southern Germany. This test site covers an area of 470 m x 615 m and is defined by the area supplied via a 630 kVA medium-to-low voltage transformer. It includes 133 households attached to the transformer via eight feeder lines (Figure 6).

Figure 6: Aerial image of the test site Einsingen. The border is marked with the blue polygon. The investigated PV-Systems with smart meters are marked in red.

At the test site Einsingen, there are 21 roof-mounted residential PV systems installed with an overall P_{nom} 233 kWp ranging from 2.2 kWp to 47.84 kWp. The average P_{nom} per roof of 11.07 kWp is close to the average value for southern Germany [38]. The PV systems are distributed over the whole test site and Landis & Gyr ZMD310 smart meters are installed at 12 PV systems providing 15 min average P_{PV} values since May 2013. The total monitored P_{nom} of the 12 investigated PV systems is 152 kWp. The tilt and azimuth angles were extracted by laser-scan data provided from a roof potential analysis for electric grid planning based on [33]. The error of these angles is assumed with less than 10°.

The irradiance data used are taken from MACC-RAD service [21]. Further meteorological data required for the simulation are air temperature and wind speed. Those values are taken from the roof-mounted meteorological station operated by Ulm University of Applied Science (latitude 48.42°N, longitude 10.00°E, height above sea level 550 m). The distance to the test site is 11 km - this is acceptable with respect to the required accuracy of temperature and wind speed in PV plant modelling. An error of 2 % in air temperature or 50 % in wind speed leads to an error in the PV yield of 0.5 % respectively 1.5 % [42].

The calculation of the P_{PV} was done for the period from May 15th 2013 to December 14th 2014 because of the availability of the smart meters provided by the DSO measurement campaign.

The scatter plots in Figure 7 shows the 15 minute averages of the time period of the simulation and measurement for each PV system. Most simulation results correlate with the main diagonal. All systems show positive biases (see chapter 0). For a better understanding three PV systems are discussed in more detail:

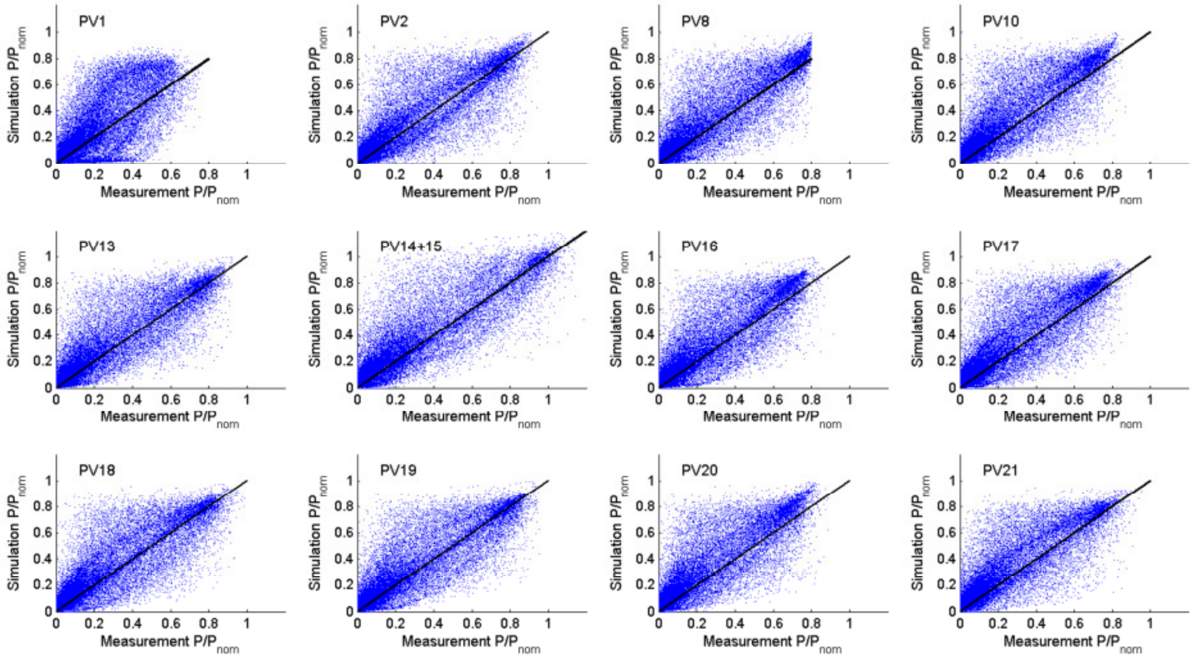

Figure 7: Comparison between measured normalized P_{PV} and simulated P_{PV} with MACC-RAD irradiance data for all 12 PV systems from May 15th 2013 to Dec 14th 2014

PV1 shows an overestimation by the simulation. The reason for this is an unusual orientation with parts of the PV modules being oriented to the East and the others to the West. The aerial image of the test site shows a majority of PV modules on the western roof. The simulation model uses a single tilt and azimuth angle for each PV system. So the East-West orientation of PV1 leads to a low correlation with real measured values.

For PV8 the measured data show an abrupt limitation at $P/P_{norm} \approx 0.78$. This could occur because of an active P_{PV} feed-in limitation of the rated power in this PV system to 0.8, due to a novelty in the German Renewable Energy Law calling for a limitation of the P_{PV} to a fraction of the P_{nom} if no device for external control is installed.

The combined PV system (PV14 + PV15) is the only system that reaches a P_{PV} of more than the P_{nom}. This system is a combination of two PV systems installed in different years on the same building and connected to the same electric meter.

All in all, the ME ranges from 0.21 kW to 0.89 kW with an additional outlier of 2.63 kW at PV1 due to its two-sided orientation. Overall, this results in a mean error of 0.59 kW. The RMSE range is from 0.65 kW to 2.27 kW with the PV1-based outlier of 7.67 kW and the overall average of 1.76 kW. The CC shows a good correlation with 0.88 and the outlier of 0.75 for PV1.

Furthermore, the ME and RMSE is normalized to the P_{nom} of each PV system to compare the results. The nME ranges from 0.03 kW/kWp to 0.06 kW/kWp with a mean of 0.05 kW/kWp. The nRMSE ranges from 0.12 kW/kWp to 0.16 kW/kWp with a mean of 0.14 kW/kWp. The normalized values show that the errors are independent of the PV system size and satisfying for residential PV simulations.

3.3.3 Influence of system orientation and irradiance source

In [43] the idea of using solar roof potential data based on airborne laser-scan data is introduced. The results of this solar roof potential contain the orientation angles for each roof and the existing PV systems. The orientation angles of existing PV systems and angles for upcoming roof-mounted PV systems can be used to improve the accuracy of P_{PV} calculation. If these angles are unknown an orientation has to be assumed which can lead to higher errors. These errors can be significant especially in small areas as low voltage grids. To study the sensitivity of system orientation and irradiance source additional simulations were performed. Four orientation angle datasets are taken into account. The first is denoted as in-situ and based on manually measurements in the test site Einsingen. The second and third angle datasets are based on the laser-scan data. The dataset denoted as “LIDAR mask” is based on a manual mask filtering the orientation data in the laser-scan results. The dataset denoted as “LIDAR window” is also based on the laser-scan data but uses the statistical approach of [33] for the estimation of the orientation. Finally, the last dataset assumes an optimal orientation of each PV system. The differences in the simulation results of in-situ, LIDAR mask and LIDAR window are minimal. The results of the calculation using the LIDAR window data are shown in section 3.3.2.

If optimal orientation (30° tilt oriented to South) for the PV systems is considered, the errors increases. The ME ranges from 0.27 kW to 0.92 kW with an additional outlier of 2.63 kW at PV1 due to its two-sided orientation. Overall, this results in a mean ME of 0.87 kW. The RMSE range is from 0.66 kW to 2.51 kW with the PV1-based outlier of 8.29 kW and the overall average RMSE of 1.97 kW. The CC is around 0.86 with the outlier of 0.74 for PV21. The accumulated P_{PV} on transformer level results in ME of 10.46 kW and RMSE of 21.33 kW, while the CC is 0.89. The nME ranges from 0.04 kW/kWp to 0.11 kW/kWp with a mean nME of 0.06 kW/kWp while the nRMSE ranges from 0.13 kW/kWp to 0.22 kW/kWp with a mean nRMSE of 0.15 kW/kWp.

As mentioned before, ground measurements are point measurements and do not fully represent the spatial and temporal variability of distributed PVs in an area. The accuracy decreases with increasing distance between the point of interest and the ground measurement [28]. The sensitivity simulation was performed using the measured irradiance data from the weather station at Ulm University of Applied Science instead of MACC-RAD irradiance data to take this effect into account for the comparison. The BHI was estimated with the DIRINT method [45] from the ground-measured GHI. When ground-based irradiance measurements from the pyranometer at Ulm University of Applied Science are used the results differ as expected. The ME ranges from -0.44 kW to -0.01 kW with an additional outlier of -1.25 kW at PV1. The overall ME is -3.61 kW. The RMSE range is from 0.61 kW to 2.2 kW with the PV1-based outlier of 7.1 kW and the overall average of 1.71 kW. The CC is around 0.85 with the outlier of 0.70 for PV1. The accumulated P_{PV} on transformer level results in ME of -3.6 kW and RMSE of 17.95 kW, while the CC is 0.85. The nME ranges from -0.05 kW/kWp to 0 kW/kWp with a mean of -0.02 kW/kWp while the nRMSE ranges from 0.12 kW/kWp to 0.15 kW/kWp with a mean of 0.13 kW/kWp.

Figure 8 shows the boxplots for the variation of the irradiance source (MACC-RAD and ground measured irradiance at Ulm University of Applied Science) and the orientation source (in-situ, LIDAR mask, LIDAR window and optimal). On each blue box, the red central mark is the median, the edges of the box are the 25th and 75th percentiles, the black whiskers extend to the most extreme data points not considered outliers, and outliers are plotted individually as red crosses. The four boxes on the left-hand side take into account satellite irradiance data from the MACC-RAD service and the four options to estimate the PV orientation angles. The P_{PV} is overestimated and the variability increases if an optimal orientation is assumed. The four boxes on the right-hand side show the results considering ground-based irradiance measurements. There is no strong bias and 99.3 % of all 15-minute data are within the range of ±20 % deviation related to the rated power.

The results show that satellite derived irradiance data can be used to calculate P_{PV} of residential PV systems in a sufficient accuracy. The errors are reduced if the real PV orientation angles are taken into account. As expected a ground based measurement nearby shows a higher accuracy.

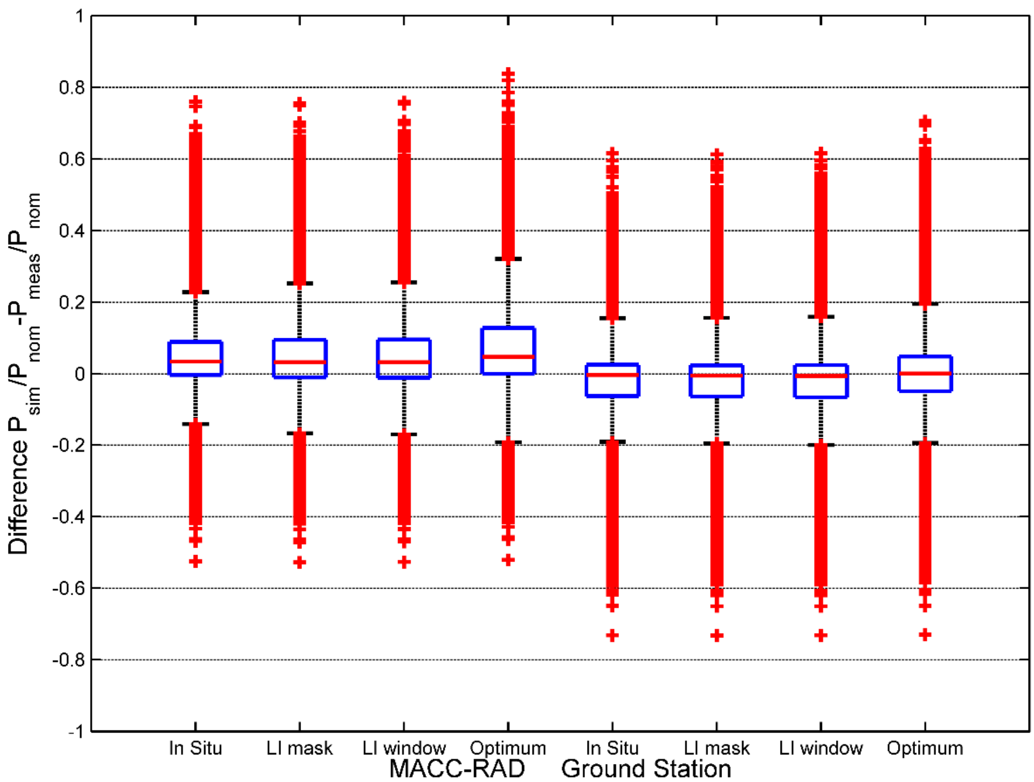

Figure 8: Boxplots of the different variations to calculate the summarized P_{PV} of the 12 investigated PV systems in 2012. The red bar shows the median, the blue boxes the 25 and 75 percentile of the data. The black whiskers extend to the most extreme data points not considered outliers. The red crosses mark the outliers. "LI" is an abbreviation for LIDAR.

3.4 Calculation of the low voltage transformer load flow with satellite irradiance data

Low voltage grids were planned for demand only. The usage of annual energy consumption, standard load profiles and drag indicators in the transformer substations were sufficient for decades as production was not part of this grid level. In the meantime, the increasing penetration of DES, especially PV systems, has changed the behaviors of the low voltage grid and has increased the need for additional information about the load flows, voltages and loadings. Based on the approach to calculate the PV feed-in power with satellite-derived irradiance, the load flow at the low voltage transformer in the test site Einsingen is calculated and validated against measurements.

3.4.1 Modeling approach

Based on the solar irradiance information, the power flow over the transformer (P_{Trafo}) can be calculated. As mentioned before, power generation by PV systems can be described with the knowledge of irradiance and air temperature – and the knowledge of the orientation and inclination of the single PV systems, the module types and local shading effects. The consumption can be approximated by load profiles e.g. statistical-based standard load profiles (SLP), synthetic-generated profiles or measured time-series.

SLP as communicated by the energy industry [46] are usually normalized to an annual consumption of 1,000 MWh and scaled up to the real measured annual consumption. Due to the statistical nature, the usage of these profiles is appropriate for clusters with at least 150 households [47]. With the 133 houses in the test area it is assumed that deviations from the German standard load profiles will be small.

The annual consumption in 2012 in the test site was 1,051 MWh, with a distribution of 85 % related to private households, 4 % to agricultural and 11 % to commercial activities. For the connected commercial and agricultural consumers the respective standard load profiles as given in [48] are used.

For the private households in the test area SLP as well as an average profile based on 145 measured load profiles (NoSLP) [17] are assumed. Both SLP and NoSLP have a temporal resolution of 15 minutes. The NoSLP profiles are from randomly selected households in Ulm, monitored from May 2009 to April 2010. Their average is re-sorted with respect to the weekdays and weekends in 2012. The influence of weather conditions on the household day to day variability is negligible. The original consumptions of the NoSLP profiles range from 0.5 MWh per year to 7.753 MWh per year with a mean of 2.739 MWh per year.

The calculation approach is visualized in Figure 9. The P_{Trafo} is given as residuum of the demanded power P_{Load} and the P_{PV}. The first line in the picture shows the calculation of the P_{PV} considering the irradiance, the PV system data and a PV model. The next step is the generation of the transformer load flow therefore the P_{load} is subtract by the P_{PV}. The last line shows the calculation of the P_{Load} based on load profiles, the annual energy consumption and an estimated grid loss. P_{Load} is approximated by using the SLP and NoSLP time series for residential customers based on their annual consumption. The corresponding SLP is used for both commercial and agricultural customers. The resulting load profile time series is multiplied by the annual consumption of the area. The annual consumption is given by the sum of the consumer energy meter values provided by the DSO [48].

The losses within the grid are estimated by a grid simulation without PV as 2.17 % of the overall annual consumption. Variation of the loss value by P_{PV} is neglected.

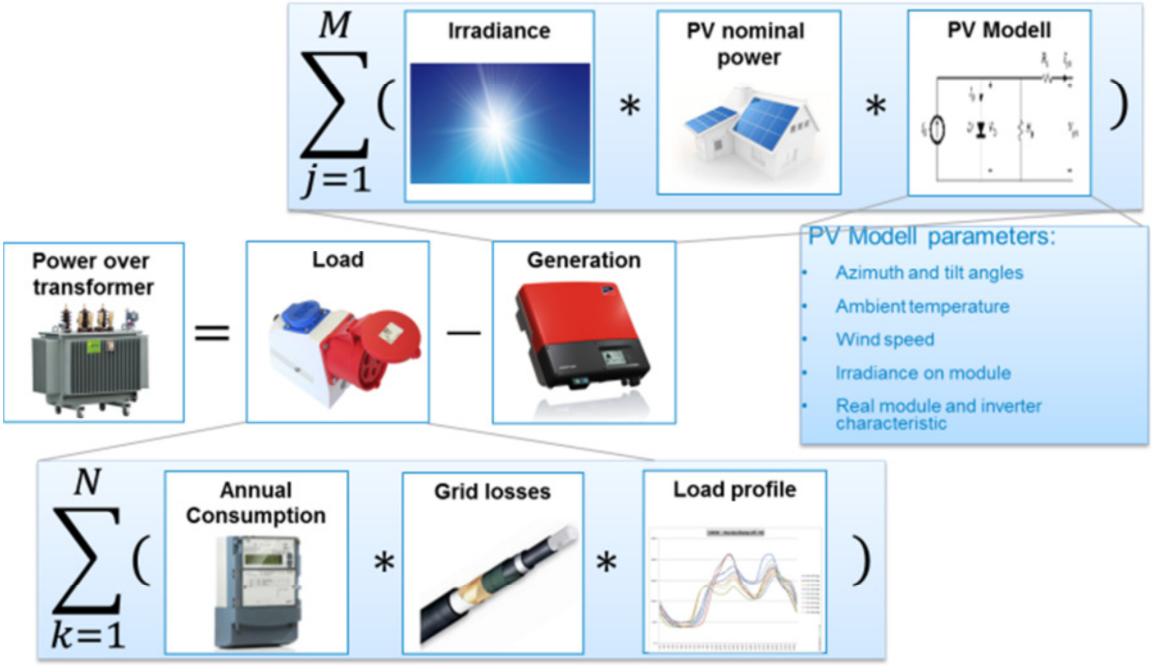

Figure 9: Visualization of the Calculation approach for the power flow calculation over the transformer.

3.4.2 Validation of calculated load flow with transformer measurements at monthly scale

The monthly rRMSE values of P_{Trafo} for the three satellite irradiance sources (see section 3.2.1) and the two load profiles are shown in Figure 10. Each irradiance source has its own bar graph. The different load profiles are illustrated as different coloured bars. As expected, there are only minor differences caused by the irradiance source. This is in line with rRMSE values of the ground-based irradiance measurements (see section 0). However, the load profiles affect strongly the rRMSE of P_{Trafo}. During the winter months all load profiles have similar rRMSE values. The rRMSE increases during the summer months.

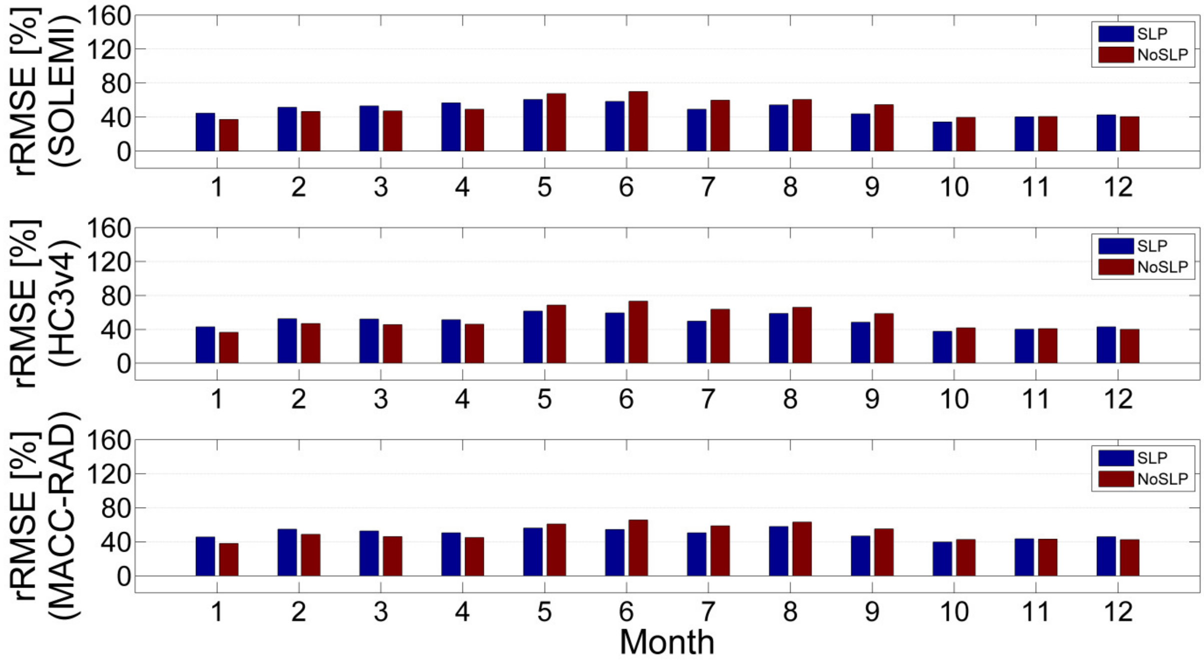

Figure 10: Monthly rRMSE values of P_{Trafo} distinguishing between irradiance source and considered load profile at the test site Einsingen in 2012.

In contrast to rRMSE, at the rME a strong variation with month, with load profiles – and to a lesser amount with irradiance source – can be observed (Fig. 11). During the summer months the rME of MACC-RAD is equal or smaller than SOLEMI and HC3v4. During the winter months the lowest rME is given for SOLEMI. February shows a negative rME for NoSLP because of unusual low outdoor temperatures below 0°C. While the multi-annual monthly average of the temperature in February is -0.1°C based on the measurement values of the years 1950 to 2013 [53], the average monthly temperature in February 2012 is with -4.2°C clearly below this multi-annual average. This cold leads to a higher consumption than assumed by the load profiles. Therefore, an underestimation occurs. The deviations between the single satellite sources are below 15 % for each month. The effects of the applied load profiles to the differences are clearer. During the winter months the rME of all load profiles are in a similar range of 20 % with lower values for NoSLP. This is different for the summer months (May to September). During this time all profiles shows increased rME. The calculations using SLP profiles are in the range of 20 to 40 % during the summer month. In the same period, the calculations taking into account the NoSLP profiles are in the range of 30 % to 50 %.

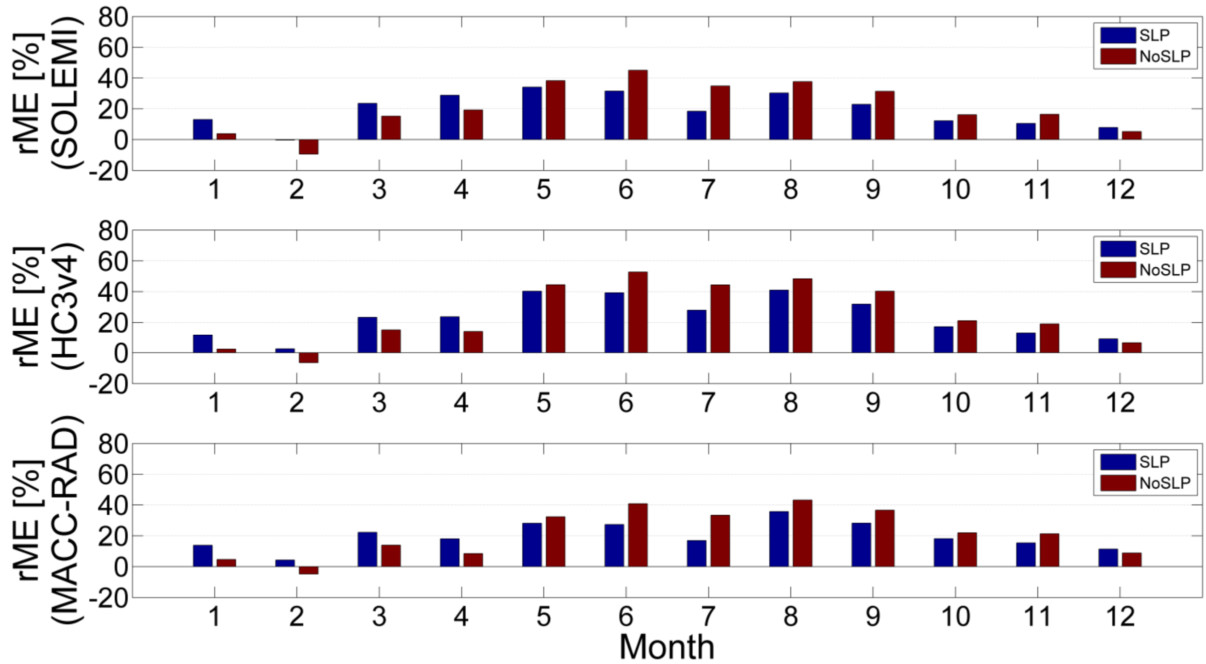

Figure 11: Monthly rME values of P_{Trafo} distinguishing between irradiance source and considered load profile at the test site Einsingen in 2012.

In terms of CC, there are no strong differences between the three satellite sources except February where CC is between 0.3 and 0.6. This is shown in Figure 12. The reasons for the outlier February is probably due to the very low temperatures and the high demand which is not considered in the load profiles (see above). In this month MACC-RAD has a CC of 0.1 points lower than SOLEMI. HC3v4 lies in the middle between both. During March to October CC has for all irradiance sources high values between 0.7 and 0.9. In the remaining months CC is in the range of 0.35 to 0.6. The consideration of the load profiles shows only minor differences between SLP and NoSLP during the period from March to October. In the winter months the difference between both SLP and NoSLP increases to 0.1. It is assumed that the load profiles do not correctly reflect the load of the test site Einsingen in the winter month. This can be caused by higher demand because of lower temperatures, the lower P_{PV} of the PV systems because of lower irradiance. Furthermore, errors in the calculation can occur due to snow on the PV systems leading to false P_{PV} values.

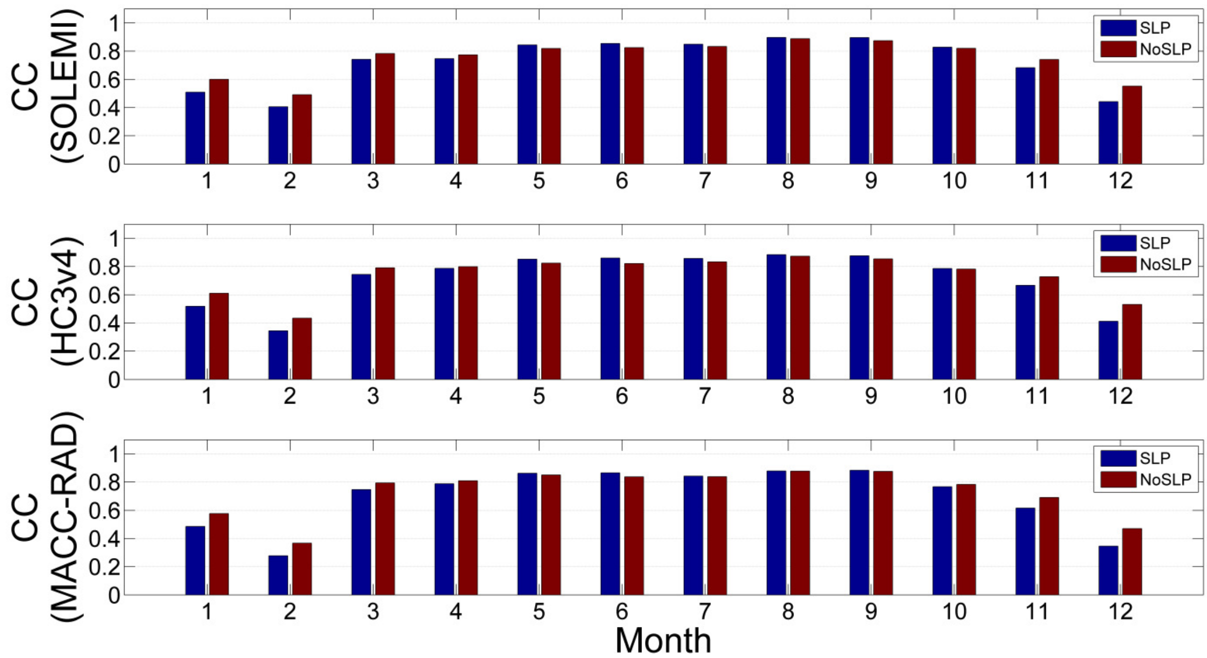

Figure 12: Monthly CC values of P_{Trafo} distinguishing between irradiance source and considered load profile.

3.4.3 Evaluation of the diurnal variation

For a better understanding also the behaviour of the diurnal variation of the load flow needs to be studied. A so called 'average day' is calculated by averaging the same 15-minute interval of each day in the observation year. This is done for the simulations variations considering the three different irradiance sources and the two load profiles as well as for the measured P_{Trafo}. DSOs have to operate the grid and are interested in the load flow over the transformer during night hours without irradiance but with continuous demand. As a consequence of the DSO´s requirements, the calculations are performed for the entire day.

The diurnal variation of the seven average days is shown in Figure 13. The irradiance data sources are distinguished by colours. The green lines show the calculated load flows using the SOLEMI irradiance data, while HC3v4 is in red and MACC-RAD in blue. Note that SOLEMI and HC3v4 data are not available during nighttime. The applied load profiles are marked with the different line types. The calculated results taking into account the SLP are printed as solid lines, while calculations with NoSLP are dashed. The black dash-dotted line represents the measured average P_{Trafo}.

The differences between the single irradiance sources are maximal 10 kW and independent from the load profile. The interpolation of the hourly SOLEMI data to a 15-minute resolution leads to oscillation effects during the day. These small deviations correspond with the comparison results of the original irradiance sources [21].

In contrast the differences between the calculated and the measured load profiles are much higher. During the night SLP and NoSLP do underestimate P_{Trafo}. The amplitude of the NoSLP is 35 kW lower than SLP at the same time. During the day all profiles follow the diurnal variations, the load flow reduction from the P_{PV} is well observable. SLP and NoSLP have higher deviations and overestimate the P_{Trafo}. The amplitude of the evening peak ~19 UTC is similar for each load profile. All profiles overestimate the measured load profile by 60 kW to 70 kW.

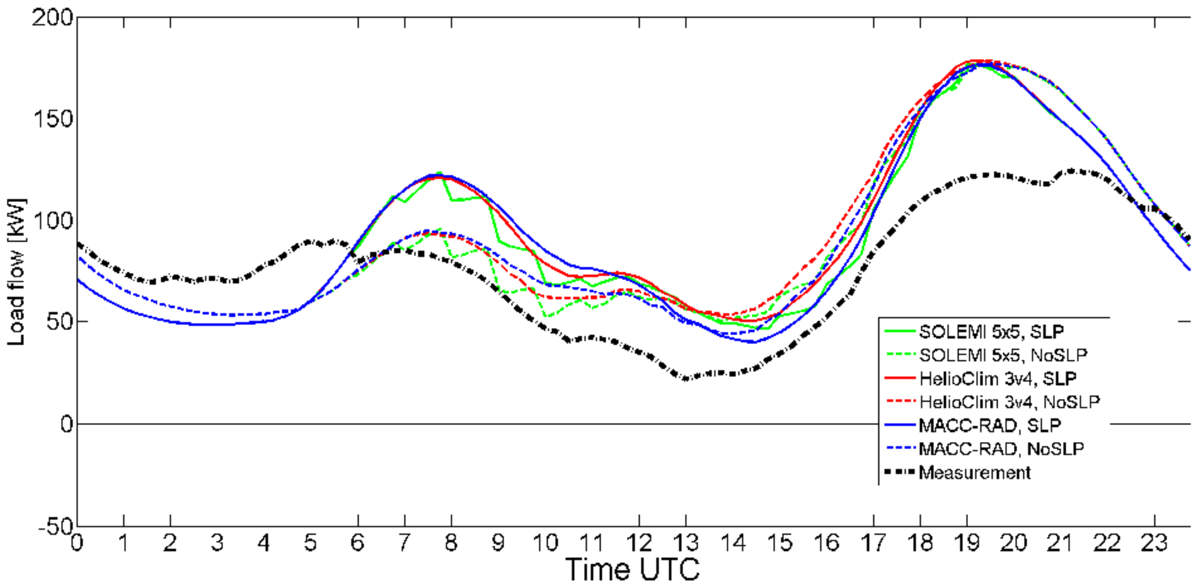

Figure 13: Comparison of calculated average load flow time series of a day against the average measurement

For each 15-minute interval of the year also the statistical measures are calculated. These statistical measures are plotted over the time of the day in Figure 14. The irradiance data sources are distinguished in the same manner as in Figure 13.

Similar to the time series of the load flow itself, the irradiance sources do not cause large deviations in the errors. The oscillation effect of SOLEMI is also visible in the ME and MACC-RAD tends to lower ME during the afternoon hours. The ME of SLP and NoSLP is below 0 during the night which means that the load flow is underestimated. The SLP profiles show a higher ME in the forenoon than NoSLP. However, the NoSLP profiles have a higher ME during the afternoon than the SLP. All profiles have their absolute maximum ME in the evening.

The standard deviation STD also do not show a strong difference caused by the irradiance sources. The HC3v4 data has a lower STD than the MACC-RAD data. The SOLEMI data has higher STD during the forenoon because the oscillation effects. The SLP and NoSLP show higher STD during the day. This is a result of the diurnal variation and depends also on the irradiance data sources.

There are no strong deviations in the RMSE curves caused by the variation of the irradiance. The RMSE considering MACC-RAD is slightly higher in the morning as for considering SOLEMI and HC3v4. The SOLEMI RMSE curve shows also the oscillation effect caused by the interpolation. In the afternoon the HC3v4 shows a higher RMSE than SOLEMI and MACC-RAD. The RMSE of SLP and NoSLP increases during the morning hours and turns to a local minimum. This local minimum is caused by the change of the ME from negative to positive while the STD is still low. During the forenoon the SLP profiles has higher values of RMSE than NoSLP. Around noon all profiles show a similar amplitude. In the afternoon the RMSE of the SLP drops to a local minimum while the RMSE of the NoSLP increases. All profiles have an additional peak in the evening around 19 UTC. The RSME of both SLP and NoSLP have the same amplitude and similar fall. The ME and RMSE curve are based on the combination of the diurnal variation of PPV and the mismatch of the load profiles. The high values during noon are caused by the high variability and amplitudes of the irradiance during the day. This leads to high RMSE and ME values in an annual statistic. The morning and evening peaks are not a result of the P_{PV}

because of its low impact related to assumed consumption by the load profiles. Basically, the CC also follows the diurnal variation. During the day the CC is in a range of 0.6 to 0.8 and during the night in the range of -0.2 to 0.4 for both SLP and NoSLP. The effects of the different irradiance source lead to small effects during the day. In terms of CC, HC3v4 performs better, followed by SOLEMI and MACC-RAD.

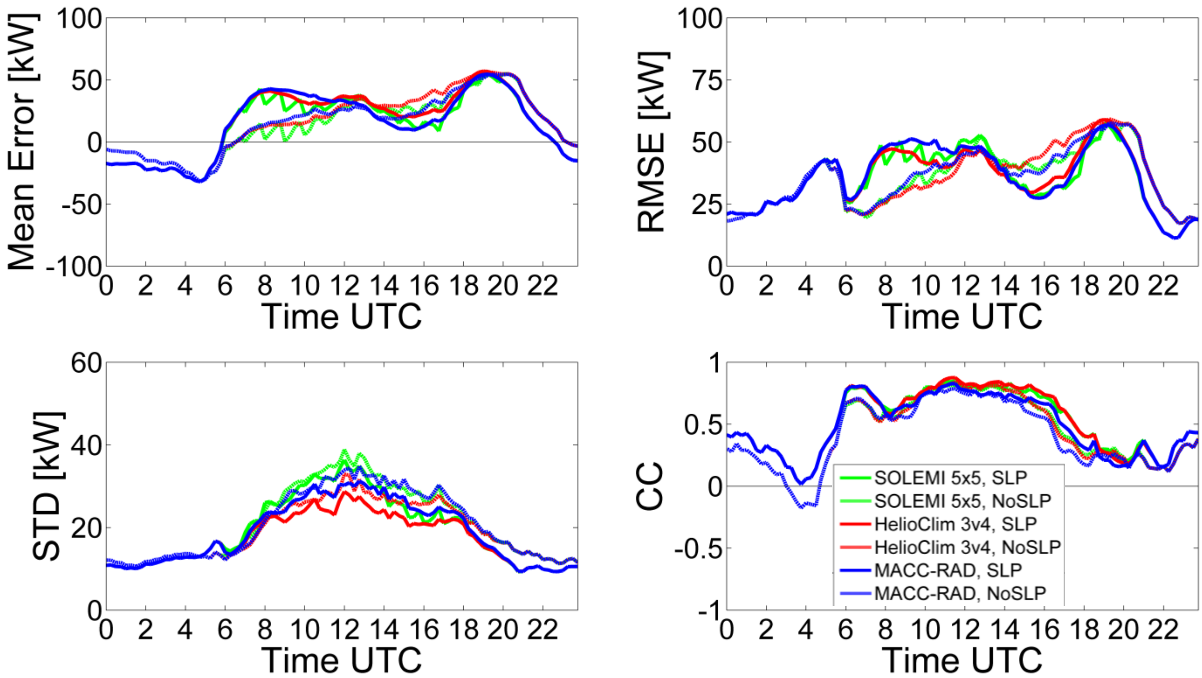

Figure 14: Variation of the PV inverter model considering a constant efficiency and SGPI model

In this chapter, the usability of satellite derived irradiance data for P_{Trafo} calculations of a low voltage transformer in a small-scale distribution grid was investigated:

The assumed load profiles have a strong influence to the results, while the different irradiance sources have only a small one. Especially, the deviation during morning and evening hours, with less PV influence, leads to high error values. The SLP shows higher errors before noon. Dealing with this mismatch between the general and statistical averaging nature of standard load profiles and the real conditions in our selected residential area is an important research question.

3.5 Calculation of the low voltage grid transformer oil temperature

Oil-immersed power transformers (OIPT) are a key element for a reliable electric supply and are planned and used for decades. The oil temperature and the resulting aging of transformers is an important factor for the asset management and have to be considered by DSO. The aging depends on the decomposition and other chemical processes of the organic parts in the isolation paper and the oil [49] and is influenced by the oil temperature. With a high number of PV systems in the distribution grid the former worst case conditions changes, from high power demand during low air temperatures in winter, to high P_{PV} with high air temperatures in summer. The oil temperature impact increases the reaction rate of the life-time consumption exponentially [50]. Therefore, the effect of the life-time consumption of the OIPT caused by high power in the summer time is much higher compared to the same transferred power at lower room temperatures.

3.5.1 Extended simulation model

The national standard DIN 60076-7 model [50] provides an aging calculation scheme based on apparent power and the room temperature values in chronological sequences. In Germany the typical distribution grid transformers are OIPT. OIPT are also the most commonly used transformer type in the grid of SWU, the local DSO in the city of Ulm, Germany [48]. OIPT are also common for private operated transformers in Ulm and therefore the simulation model is based on the guide-lines of the DIN 60076-7. Most of these OIPT are housed in standardized buildings. However, a detailed consideration of these housings of the OIPT is not part of the DIN 60076-7. To calculate a more accurate room temperature based on available metrological parameters, it is necessary to add an additional building model and extend the DIN 60076-7 model.

Aging of OIPT is described by the life-time consumption for which the hottest-spot temperature has to be evaluated. The hottest-spot temperature is the temperature with the highest temperature value in the oil and it is influenced by the transformer load factor K. The factor K is given by

$$K = \left| \frac{S_{act}}{S_{nom}} \right| \tag{9}$$

where S_{act} is the actual apparent power and S_{nom} is the nominal apparent power of the OIPT. A higher K gains more stress to the OIPT and increases the live-time consumption. Typically, DSO evaluates OIPT with a max K value of nearly 0.8 within a year as heavily loaded.

The room temperature assumed by DIN 60076-7 is not equal the room temperature of the OIPT. There is only the possibility for the use of a simplified assumption or local measurements. Nevertheless, room temperature measurements are not common in a transformer station.

The proposed approach solves this issue by an additional 'layer' around the already existing power transformer model considering further relevant power flows. Figure 15 shows a schematic visualization of these power flows and parameters. The dynamic input parameters are the load factor, the solar irradiance, the air and the soil temperature.

In addition to the supplemented transformer model the P_{Load} and P_{PV} has to be determined and summed up to calculate the load factor K.

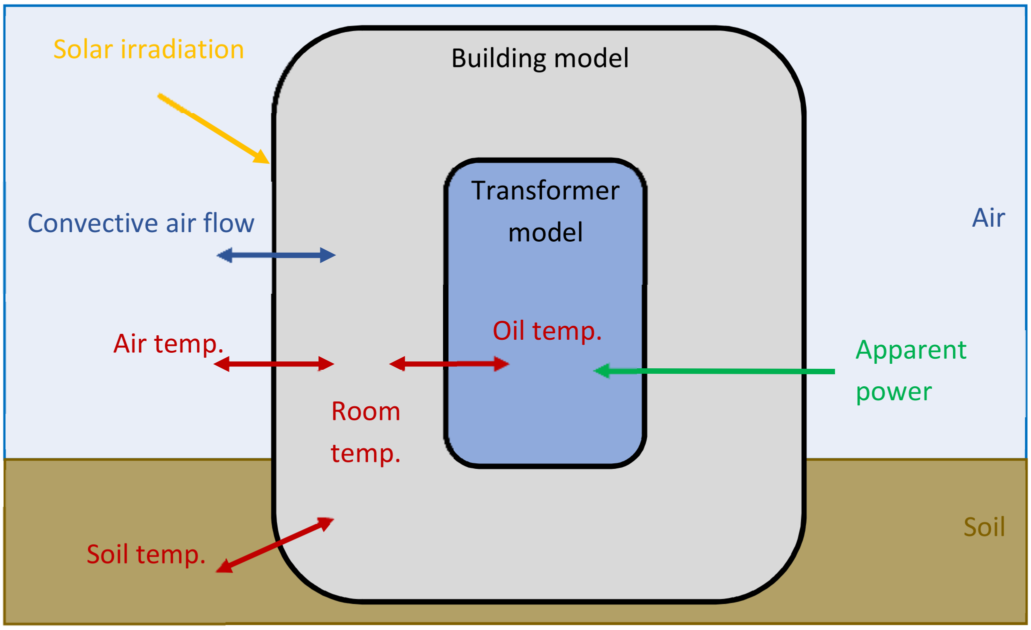

Figure 15: Schematic visualization of the interaction of the input parameters to the room and the oil temperature

The transformer model is implemented according to DIN 60076-7 and the internal parameters are set to the suggested values for distribution power transformers. The time constant which describes thermal behavior of the transformer windings is the fastest process to be modelled with a suggested time constant of 4 minutes.

Nowadays, new transformers, switchgears and the related assets (e.g. breakers and measurements) are housed in a standardized-type building. As the number of these similar stations increases the stations can be described with a low number of building models. The static parameters of the building model are calculated based on constructional drawing and material constants.

The following three physical processes lead to a change in the room temperature of the building:

- Transmission heat flow (red arrows in Fig. 17)
  The transmission heat flow is calculated based on the building plan. In this case the physical characters of the building materials are described in [51], [52]. The dynamic parameters for this model are the air and soil temperatures [29], [53].

- Convective air flow (blue arrow in Fig. 17)
  The convective air flow has a strong influence on the room temperature of the OIPT and is a common cooling solution for OIPT in standard type housings. The air flow depends on the temperature difference between the room and air temperature and the wind speed and direction. The temperature difference causes a difference in the air density. These gain, after the Archimedes principal, a lifting force to the air molecules and move them. The influence of the convective air flow by wind, is driven from the resulting pressure difference on building surface where the wind comes from and the counterpart surface. For a calculation is the wind situation for the building necessary. This is strongly influenced by the building surrounding environment. With the available database is an analysis of these effects very difficult. For this simulation a very simple model based on the air temperature and the room temperature is used [54]. Other physical parameters involved in the calculation are the height difference between the air in- and outtake, the section profile of the air in- and

outtake, the density of air depending on its temperature and the specific thermal capacity of the air.

- Solar irradiation (yellow arrow in Fig. 17)
  The solar irradiation generates an additional heat source and especially occurs in the critical summer time. To estimate the irradiance on the walls of the building the azimuth and elevation angle [30] and the specific GHI from a nearby weather station [29] are taken into account. With the knowledge about the geometry of the building and the absorption of short wave irradiation by concrete and aluminum it is possible to calculate the solar heat power flow for the building.

The outcome of the simulation is a time series of the hottest-spot temperature as well as the relative lifetime consumption. The relative lifetime consumption is related to the nominal operation conditions and is described by an exponential equation. The actual hottest-spot temperature is corrected by the nominal hottest-spot temperature for the reference life-time consumption to gain the hottest spot temperature. In Table 2 this calculation results are shown to demonstrate this relation. The increase of temperature – especially above 116°C – leads to a strong increase of relative lifetime consumption of the OIPT.

Table 2: Hottest spot temperature influence to relative life time consumption

Hottest spot Temperature [°C]	92	104	110	116	122	140
Relative life-time consumption	0,125	0,5	1	2	4	32

3.5.2 Application in the test site Ulm

At the test site Einsingen (Fig. 8) there are 21 roof-mounted residential PV systems installed with an overall P_{nom} of 233 kWp, with a systems range from 2.2 kWp to 47.84 kWp. A measurement device logs the voltages and load flows per second for each single feeder at the transformer with an accuracy of 4 %. The modelling of the recent situation is based on the measurement data from 1st January to 31th December 2012 in aggregated format to fit the simulation step size.

The simulated P_{PV} is based on the grid simulation tool DIgSILENT PowerFactory 15.2. The potential for further PV system installations are taken into account based on [43]. At the current status the PV roof potential is utilized by only 14 %. In Table 3 the P_{nom} of the calculation scenarios are shown and the share of the overall potential capacity is listed.

The P_{PV} for the scenarios with +25 %, +50 %, +75 % and +100 % of the remaining roof surface is simulated. The name of the scenarios describes the analyzed additional PV potential in percent. These defined scenarios in this chapter are different from the OrPHEuS base line Scenarios. The calculation of the load-only scenario is performed by summate the simulated P_{PV} and the measured P_{Trafo}.

Table 3: P_{nom} for PV system according to the potential in the different potential scenarios. These scenarios are denoted with the percentage values.

Scenario	P_{nom} [kWp]	Percentage [%]
Only Load	n/a	0
Current situation	232,6	14
+25%	596	35
+50%	960	57
+75%	1324	78
+100%	1688	100

The Carpet plots shown in Figure 16 are used for a more detailed look into the hottest spot temperatures of the different scenarios. The x-axis shows the days of the year and the y-axis show the hours of the day. The hottest spot temperature is scaled on the colour bar from 0° C to 110° C. The upper limit was set to 110° C as this is the nominal value for thermal stabilized oil impregnated paper and the nominal lifetime consumption, see Table 2. The carpet plots visualize the hottest spot temperature for the problematic time slots in the analyzed year 2012. The highest air temperatures for all scenarios are reached in summer at noon and the hottest spot temperature decreases only slowly during the night. There are still hottest spot temperatures in excess of 40° C in the late night. While the air temperature typically reaches its lowest values in the early morning hours and is under the 40° C value, also in summer (not shown). In scenarios with a high PV penetration (+50%, +75% and +100%) swift high temperature values more and more in the night time. While the temperature difference between max and min value degrees, also in winter. To handle these new temperature conditions are different cooling systems necessary.

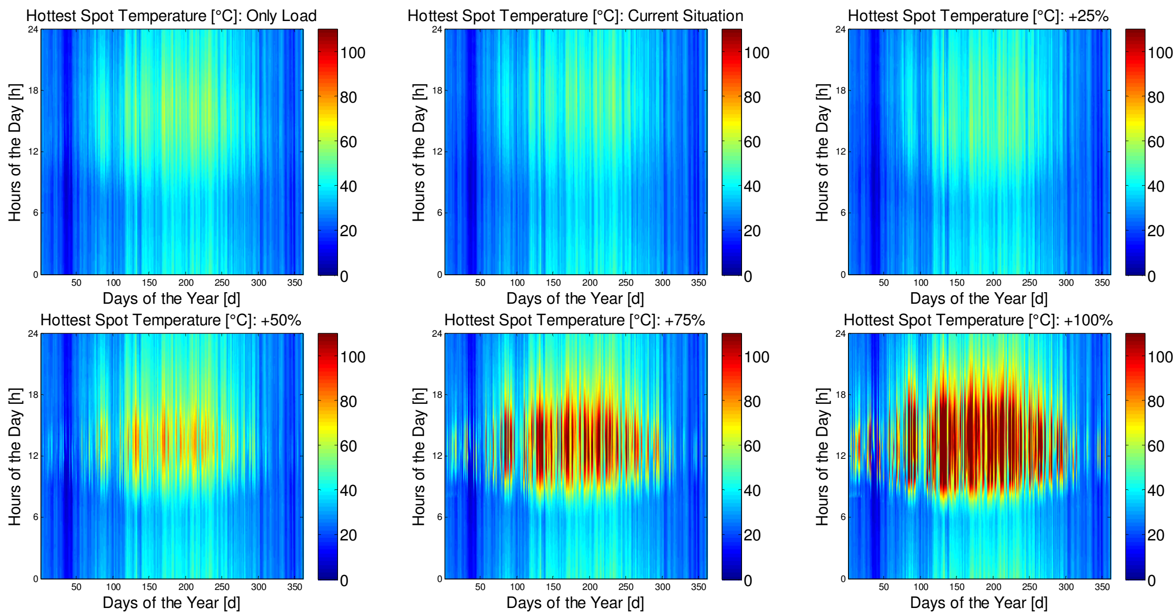

Figure 16: Carpet plots of the hottest spot temperature in the six scenarios with consistent scaling of the colour bar in 2012

A more detailed comparison between the scenarios is done in Figure 17 to illustrate the fluctuations in temperature / lifetime consumption. For one week in January (top plot) and one in August (base) the lifetime consumption is shown in high temporal resolution. Note: as the variability of the consumption is very high, the curves are on logarithmic scale. The "base load" of the life-time consumption during summer (~10^{-4}) is ten times higher compared to the winter (~10^{-5}). In winter season there are fewer peaks probably due to lower irradiance values caused by cloudy conditions and they also have a lower magnitude. Especially the comparison between the consecutive days 27 and 28 shows the enormous difference in the lifetime consumption for the scenarios above +25% (difference in order of 10^5)

Figure 17: Seasonal comparison of the characteristic for a summer and winter week in 2012.

Figure 18 shows the seasonal influence with the higher summer air temperatures and the higher solar irradiance for the six different scenarios which are indicated by the different coloured bars. The logarithmic scaling of the y-axis gives a clear impression how strong the scenarios and months differ. The scenarios with a high PV penetration show a sharp increase of the lifetime consumption. This is directly linked to the high hottest spot temperatures as shown in the carpet plots (Figure 16). The 'current situation' and '+25%'-scenarios with low PV penetration show a reduction in life-time consumption. The cause of this effect is the local balancing between P_{Load} and P_{PV}.

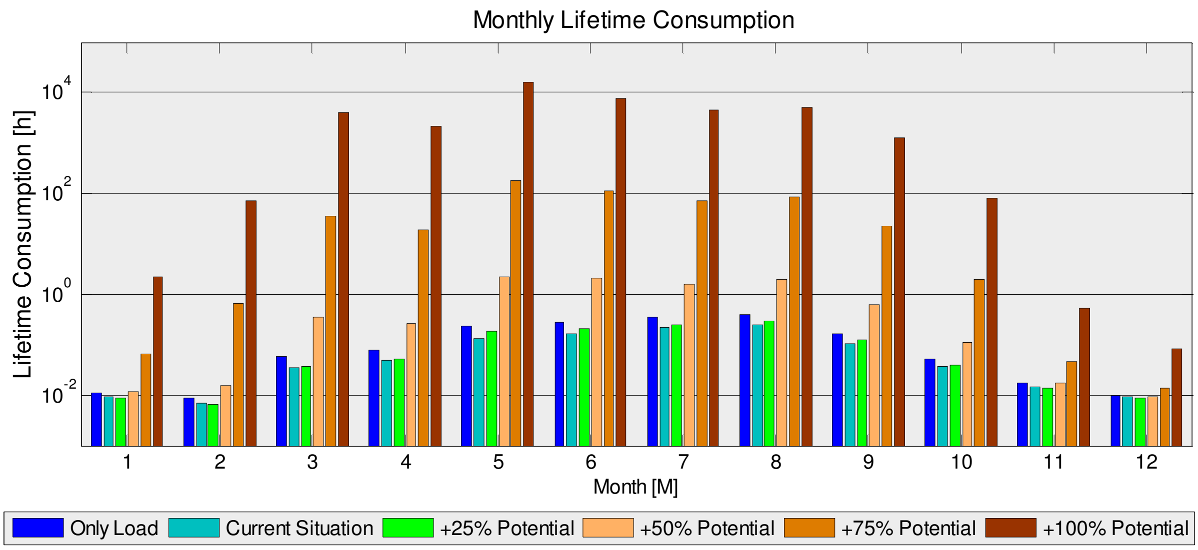

Figure 18: Cumulated monthly lifetime consumption for the six scenarios on a logarithmic scaling of the y-axis.

Figure 19 shows the load factor K of the OIPT for the complete year. The factor K of the scenario 'Only Load' is for all months higher than in the scenarios 'current situation' and '+25 %'. Therefore, a higher K in an only-load scenario allows implementing more PV systems without negative effects to the aging of the OIPT. The occurred load factor in the max scenario ´100 %´ reaches in the max 1.8. This value is theoretical for a short time, with strong life-time consumption from the transformer to handle [54]. However, the simulation shows also in Figure 16 that the maximum temperature limit of 110 °C is violated. The PV influence is only approximately four month of the year given.

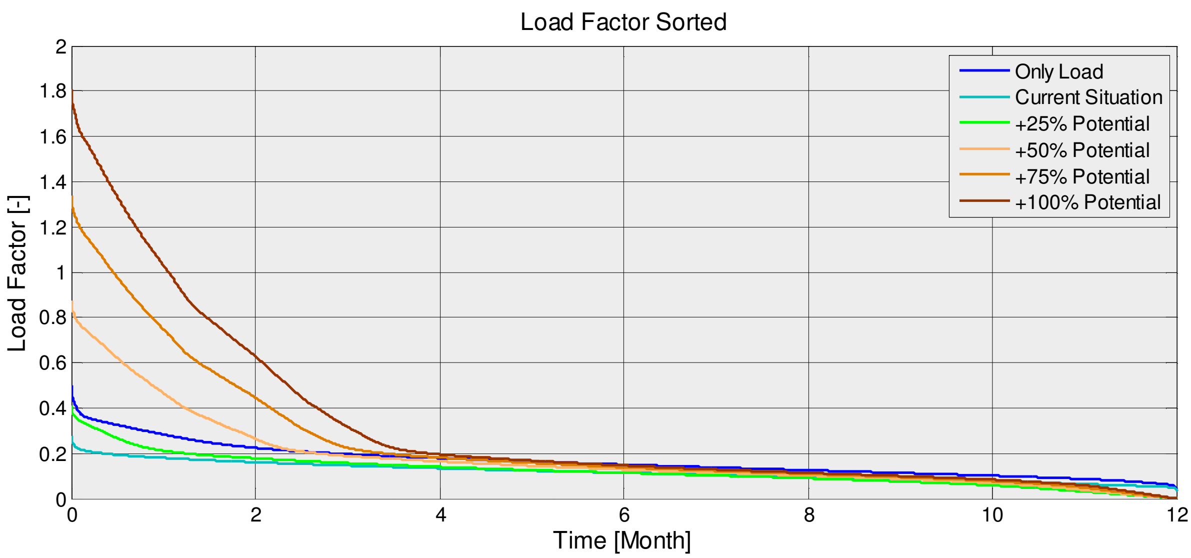

Figure 19: Sorted annual load factor curve for the six scenarios in a descending order

3.6 Correlation of transformer voltage drop and clouds reducing the irradiance

The low voltage grid and the medium voltage grid have a fixed coupling caused by the missing controllable elements. Nowadays, controllable transformers are commercially available for the low voltage to medium voltage coupling. These transformers could perform tap changes during the operation under load. However, they are not commonly used, so their impact to hybrid grids has to be investigated in future while here the strong coupling by regular transformers is investigated. The P_{PV} inside a grid area increases the voltage. Depending on the ratio of generation and consumption the P_{PV} can exceed the local power demand and the surplus results in a reversed P_{Trafo} from the low voltage to the medium voltage grid. This local feed-in increases the voltage at this point in the medium voltage grid again. So the local generation can affect the medium voltage grid. Vice versa, the medium voltage grid also affects the low voltage grid. Changes in the medium voltage grid configuration caused by switching activities or tap changes in the controllable high voltage to medium voltage transformers in the substations lead to changes in the voltage level for each area connected to the medium voltage feeder.

The effects and correlation between the P_{PV} and the ambient parameters like irradiance and clouds are investigated using the measurements in the test site Einsingen. Especially passing clouds have a strong effect on the irradiance and on the P_{PV}. As mentioned before, the P_{PV} and the power consumption results in the residual power flow at the transformer. The power amplitude mainly depends on the electric current in the public grid. A voltage drop occurs because of the impedance of the lines and assets. The amplitude of the voltage drop varies with the electric current variation and therefore with the power flow. High amplitude of power causes a high voltage drop. The following section investigates the correlation between clouds above the test site Einsingen and the voltage drop along the transformer.

The change of the active power over the so-called bus bar connecting all feeders at the low voltage transformer and the corresponding voltage change is shown in the scatter plots in Figure 20. The plot on the left-hand side shows the results from January 2012 while July 2012 is visible in the plot on the right-hand side. The diagonal trend is the consequence of the local power flow and the resulting voltage change at the transformer. It reaches values of 1.5 V/min with a corresponding active power change of 40 kW/min (visible at the left site). This trend increases during the year and a seasonal effect caused by the PV production is assumed. The influence of the medium voltage can be easily seen in the vertical trend of the scatters in the middle of each plot (red box). There are significant voltage changes up to 4 V/min while the active power changes are approximately 0 kW/min. The figure is based on the measured voltage and active power at phase 1 of the bus bar.

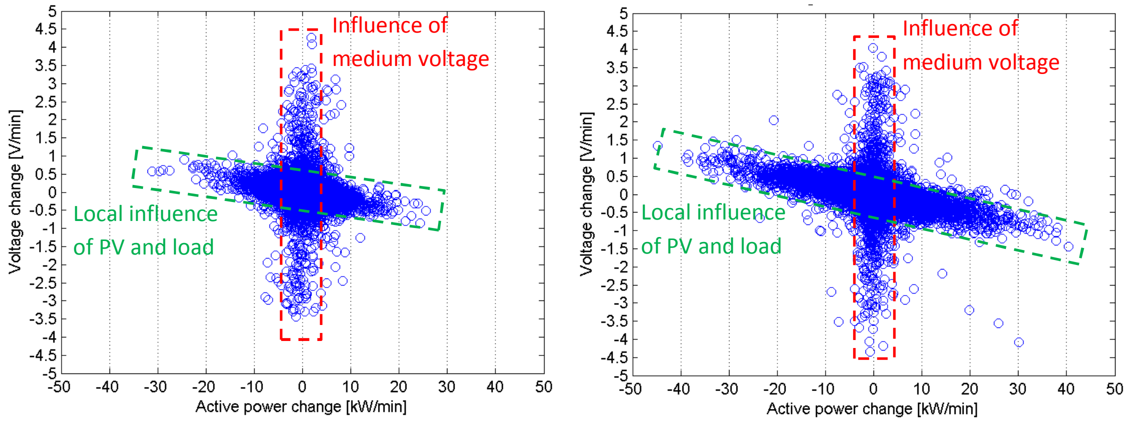

Figure 20: Scatter plots of active power change over the bus bar of the low voltage transformer and the corresponding voltage change in January 2012 (left) and July 2012 (right).

However, it is hard to distinguish between voltage changes because of a local P_{PV} variation caused by cloud passing and the naturally variation caused by the connected consumers. The measured curves of the voltage even do not show a similarity during clear sky days. Figure 21 shows three curves in minute resolution of different clear sky days. Each curve shows a working day: the green and blue curves are two consecutive days in April 2011 and the red curve is a working day in August 2011. The August values differ strongly from the April values, a similarity is not visible. The two consecutive days (blue and green lines) shows a temporal common maximum around 10 UTC but from ~11:30 UTC also these two curves diverge. The fast voltage change at 14:00 UTC in the red curve shows the effect of a tap change action in the medium voltage and the resulting effect on the low voltage site. Thus, the raw voltage measurement values from the bus bar are not usable to find a correlation to the cloud information.

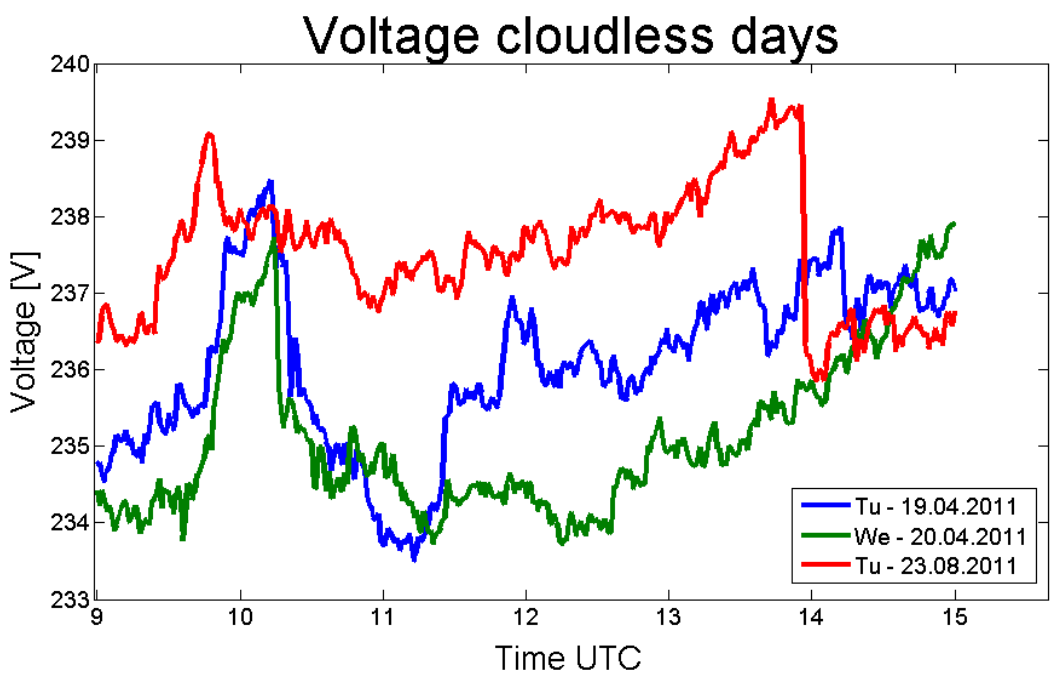

Figure 21: Comparison of voltage time series for three clear sky days.

Therefore, the load depending voltage drop at the transformer is investigated regarding cloud influences. This voltage drop depends only on the P_{Trafo} which is related to the P_{PV}. The consumption of both powers is independent of the voltage of the medium voltage grid.

DLR's cloud APOLLO product [56] is used as cloud information. APOLLO derives cloud mask and cloud physical parameter products from the MSG satellite images. The APOLLO methodology delivers cloud mask, cloud classification, cloud optical depth, and cloud top temperature as cloud parameter products for each MSG SEVIRI pixel in a temporal resolution of 15 minutes during daytime, for the period 2004-2012 (8 years). The covered zone is [60°N,60°S,60°E,60W] with a spatial resolution of 3x3 km^2 at the nadir of the satellite [0°, 0°] and of about 4x5 km^2 to 5x6 km^2 in Europe.

The cloud type allows to distinguish thin cirrus clouds with a small optical depth from (at most times) optically thicker water or mixed phase clouds. This is important for a correct interpretation of the behavior of PV to the voltage. Thin ice clouds have only a small extinction to the GHI, so the influence of PV could be underestimated if only the cloud mask were used to detect cloudy/cloud-free days.

To analyze the impact of clouds to the P_{PV} and the related voltage drop at the low voltage grid transformer two types of days are taken into account: clear sky and overcast days. The selection was done by analyzing the cloud type of each day. A Clear sky day is defined with more than 90 % of the daytime of cloud type 0 (cloud free). The overcast days is defined with a more than 90% of the daytime of cloud type 5 to 7 (low, medium and high clouds). This definitions and the quality check for full measurement datasets leads to 32 clear sky days and 42 overcast days in the time from April 2011 to December 2011. A full measurement dataset comprise a clear or overcast sky with no missing measurement data from the satellite or the transformer measurement. Days with changing cloud conditions are not in the focus of this work but will be investigated in the future.

The results are expressed as voltage rise which means the reduction of the load-driven voltage drop at the transformer and are shown in Figure 22 for all days [57]. The solid lines shows the mean values of clear sky (red) and overcast (blue) days while the dotted lines indicates the range of the standard deviation. There is a clear gap between the clear sky and overcast voltage rise. The installed PV systems reduce the load driven voltage drop over the transformer on clear sky days by 2 % p.u. in the average. There is also a reduction of the voltage drop during the overcast days. For cloudy days this reduction is in average down to 0.5 % p.u. only. During the night hours of overcast days the measurement shows a negative bias. This means that the consumption during night is higher than the used standard load profile expected.

The investigation shows the PV-driven dependency of the grid voltage and irradiance. The dependency can be expressed with cloud indicators used for the understanding and estimation of the bus bar voltage at a low voltage distribution transformer. It rejects the influence of the medium voltage by using the voltage drop over the transformer as quantitative measure instead of the absolute voltage.

Further analysis will investigate the voltage drop during days with changing cloud conditions as well as the influence of the PV penetration rate at a distribution transformer. The scatteredness of the surrounding cloud field will be taken into account as well. This will help to understand the local effects of PV to the voltage in the low voltage grids and can be used to define new guidelines for the grid planning.

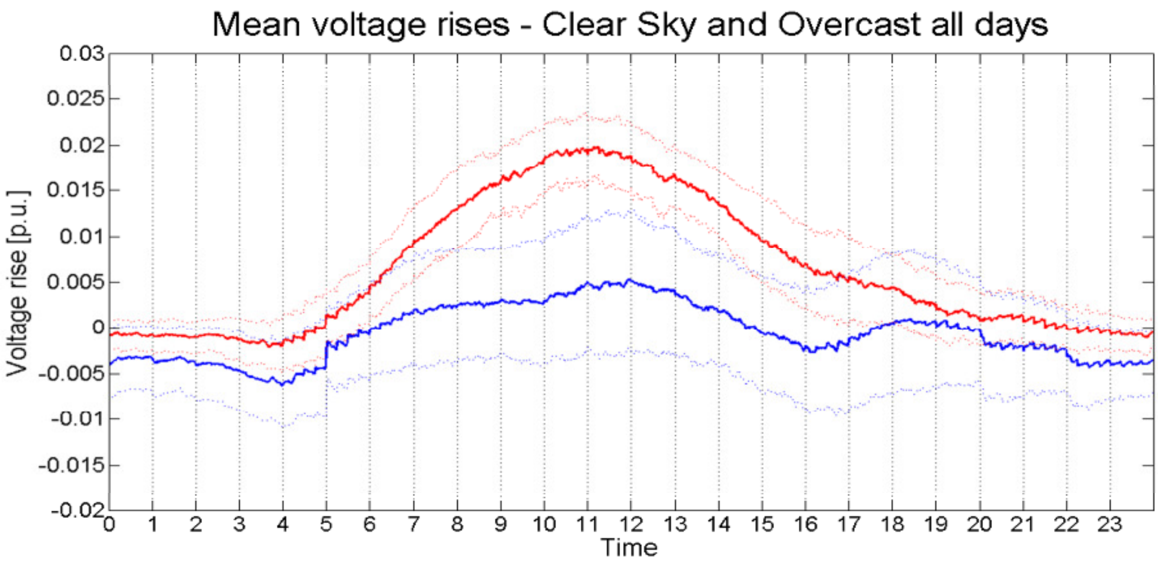

Figure 22: Calculated voltage rise on clear sky (red) and overcast days (blue). The bold lines show the mean of the used dataset days while the thin lines show the standard deviation.

4 Air Temperature

4.1 Overview

The main impact factor for heating related energy grids e.g. district heating or gas grids is the air temperature. Furthermore, also the efficiency of PV systems depends on the air temperature. When the air temperature increases the efficiency of the PV modules decreases and reduces the P_{PV}.

The air temperature is measured in 2 m height at defined points in high accuracy by meteorological stations. These stations are operated from meteorological service providers (national or commercial), research institutes or utilities. These measurements result in time-series of air temperatures at a single location influenced by the local circumstances as micro-climate or elevation.

Furthermore, meteorological re-analysis techniques provide air temperatures with a lower spatial resolution but over a large area [60]. Such a re-analysis uses the same numerical weather prediction as in weather forecasts, but is run for an historic episode and does only perform the analysis step and omits the forecast step. The air temperature data used in the following comparison were extracted from the Modern-era retrospective analysis for research and applications (MERRA, NASA) dataset provided by www.soda-pro.com. The dataset contains wind speed and direction, air density and air temperature. While air temperature is related to 2 m above ground each other values is related to 10 m over ground. Being a global numerical weather prediction model, the dataset has global range, but a low spatial resolution of 0.5°x 0.66°.

The MACC-RAD service uses the forecasts of European Center of Medium Weather Forecast (ECMWF) for the aerosol content of the atmosphere. The accuracy of these forecasted air temperature values is investigated with help of the measurements of 35 DWD ground stations in Germany (s. Figure 2).

According to Krauter et al. [61] an error in the air temperature of 1°K leads to approximately 0.5 % change in power at the maximum power point P_{MPP} of the PV modules.

4.2 Intercomparison of the various datasets

This section validates the different air temperature sources (not WMO-conform stations, MERRA reanalysis and ECMWF forecast) with ground measurements of WMO-conform weather stations. The validation of the small-area comparison is done with the stations at the demo site Ulm. For the MERRA dataset validation both Ulm and Skellefteå are taken into account. The ECMWF intraday air temperature forecast values are compared with 35 ground measurements in Germany.

4.2.1 Comparison of temperature at ground station Ulm with reference meteorological station

The demonstration site Ulm provides different sources for temperature measurements. Until September 2014 the DWD operated a weather station in the south-west of Ulm. The DWD station was then transferred to a new location in Ulm-Mähringen and is in operation since 1st September 2014. HSU and SWU each operate a weather station in the north of Ulm while SWU has a further station “Senden” in the south-east with a larger distance to Ulm. The position of the weather stations as well as the two test sites in Ulm are shown in Figure 23. Each station measures the air temperature. The location of the new DWD station is not shown because it is outside the map.

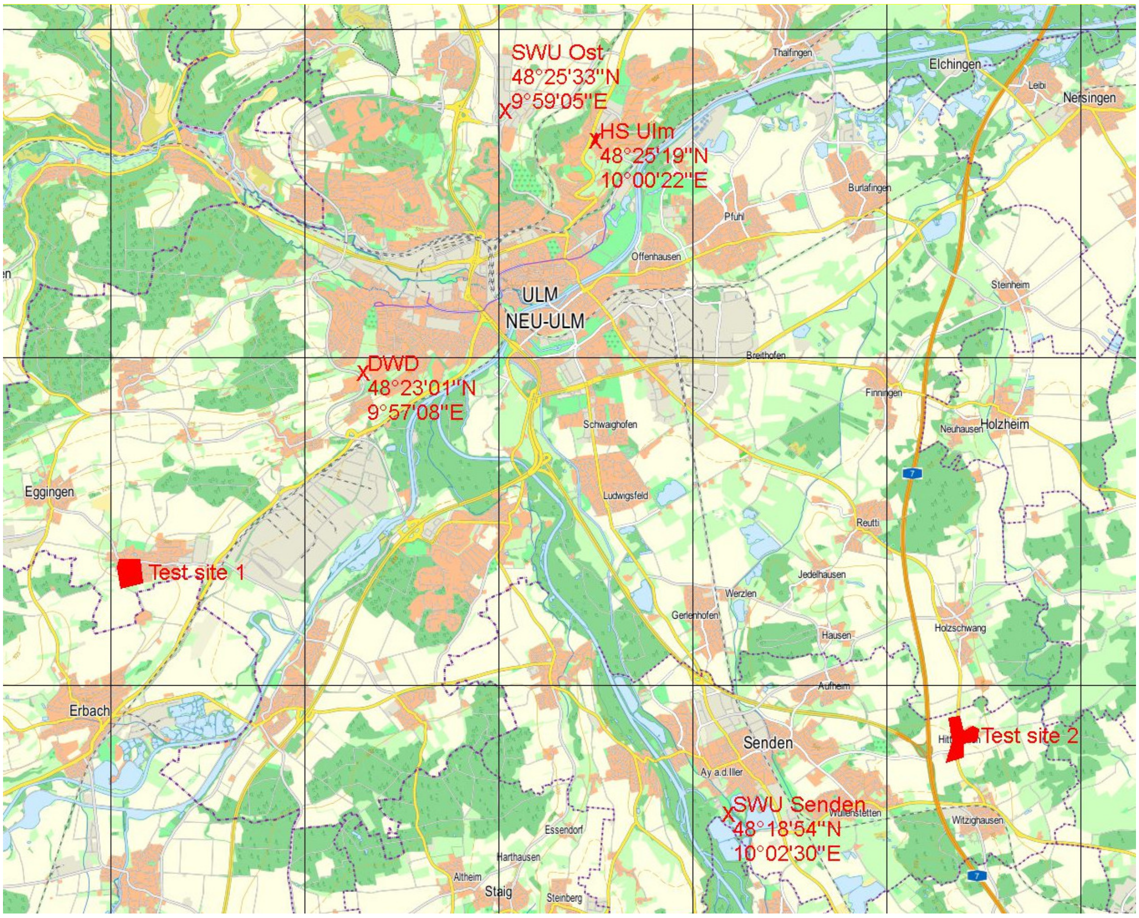

Figure 23: Available meteorological measurements in the demo area Ulm, Germany

Figure 24 shows the temperature scatter plot of the meteorological stations of the DWD versus of HS Ulm. The main diagonal is shown as the chain dotted line and indicates a perfect measurement without error. All measurements follow and scatter around this main diagonal. The frequency distribution is given by the different colours. Red means high frequency while blue means rare occurrence. The red solid line shows the regression line. The comparison of the air temperature shows a strong correlation (ME = 0.01 K, RMSE = 0.58 K, CC = 1.00). Therefore, the data of the university station can be assumed as accurate because of the low error values and high correlation.

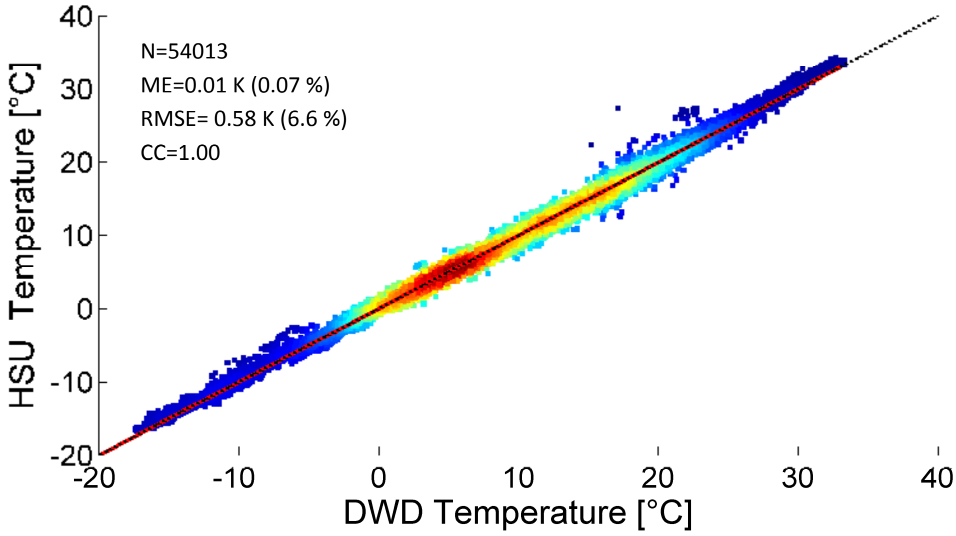

Figure 24: Comparison of air temperature measured at the meteorological stations of DWD and HS Ulm, Germany. The frequency of occurrence is colour-coded: blue low frequency, red high frequency.

In June 2014, a compact weather station was mounted at the transformer station located at the test site and is used for the comparison of air temperature and wind speed between the weather station at the university campus and the test site. The results are an indicator for the deviation because both university campus and test site do not correspond to the WMO guidelines for weather stations. The reason for the comparison of these two stations is the availability of the GHI and high time resolutions at both locations. Air temperature as well as wind speed and wind direction at the test site are provided by a Vaisala weather transmitter WXT520 using an ultrasonic transducer to measure the wind speed. The accuracy of the weather transmitter is stated as ± 0.3 K at a temperature of 20°C.

Figure 25 shows the air temperature scatter plot of both the meteorological station at the test site Einsingen and the meteorological station of HS Ulm. The main diagonal is shown as the chain dotted line and indicates a perfect measurement without error. All measurements follow and scatter around this main diagonal. The frequency distribution is given by the different colours. Red means high frequency while blue means rare occurrence. The red solid line shows the regression line. The air temperature also shows a strong correlation (ME = 0.35 K, RMSE = 1.92 K, CC = 0.97). Very low air temperatures are overestimated by the HS Ulm station. This can be an effect of the different elevation, surrounding buildings and other effects to the local micro climate.

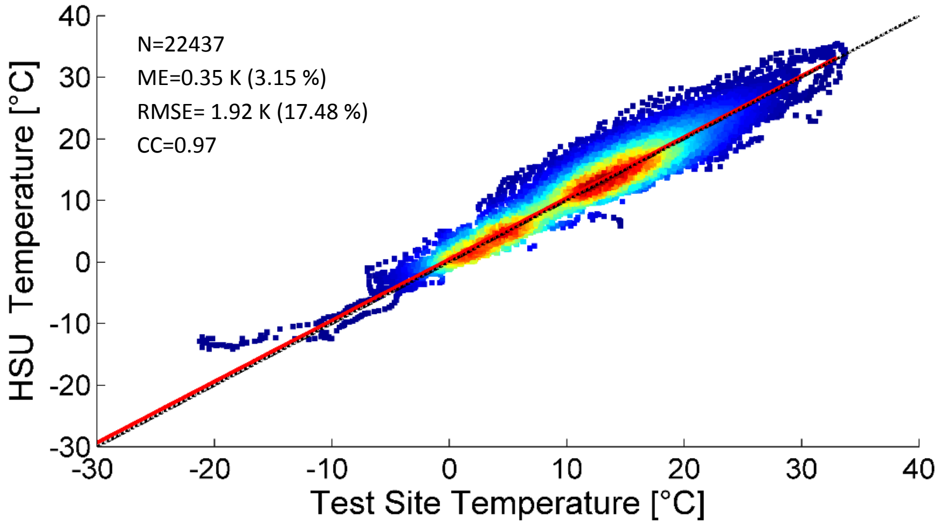

Figure 25: Comparison of air temperature measured at the meteorological stations at the test site Einsingen and HS Ulm, Germany. The frequency of occurrence is colour-coded: blue low frequency, red high frequency.

4.2.2 Validation of MERRA temperature values with ground measurements

The ground measurements show a good agreement for the demo site Ulm. However, this cannot be assumed for other locations without further investigations. Local effects e.g. microclimate or bad sensor locations can lead to offsets and higher variability. Therefore, remote sensing and forecast data are evaluated.

In Figure 26 is the result from the MERRA dataset provided by [30] referenced to the HSU dataset. The analysis considers the years of 2012 to 2014. The MERRA data have a higher negative bias compared to the ground measurements of more than -0.05 K and a RMSE of almost 2.4 K. This is in agreement with the well-known fact that coarse spatial numerical weather prediction - as in MERRA - are capable to reproduce the day-to-day variability very well, while they show also a bias [62]. The bias is typically representing the difference between the local measurement station characteristics and the MERRA 0.5° x 0.66°-grid box average being representative as average for a larger area.

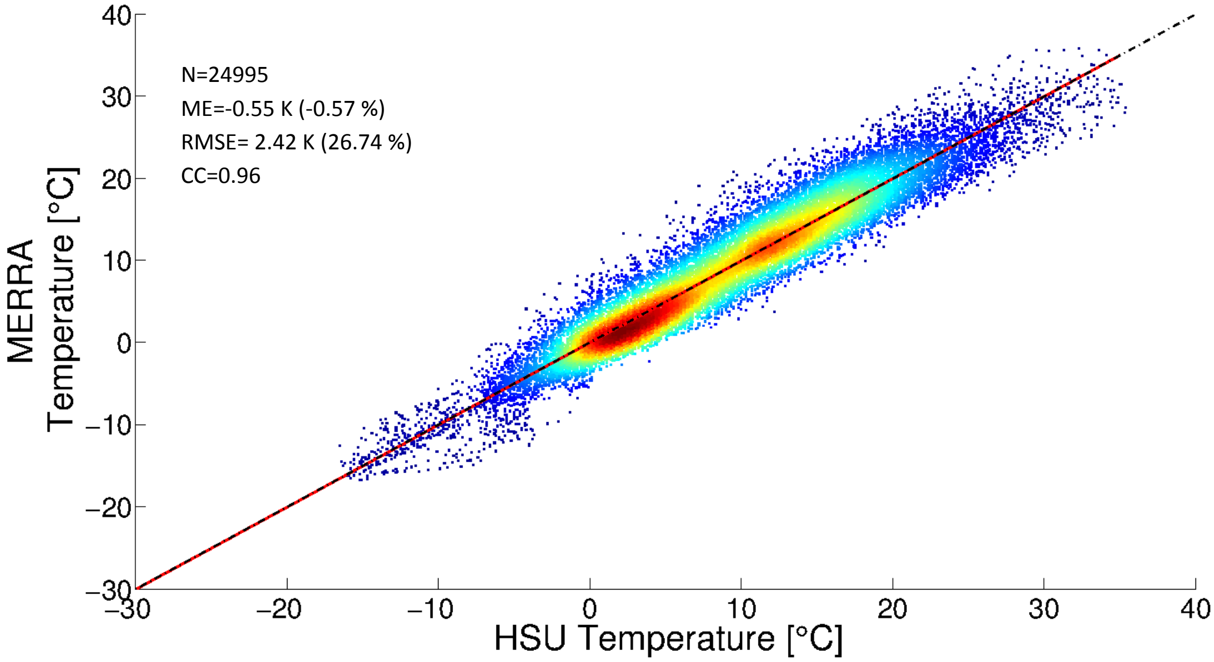

Figure 26: Scatter plot for comparison of MERRA re-analysis data versus a ground measurement of HS Ulm weather station. The frequency of occurrence is colour-coded: blue low frequency, red high frequency.

For the demo site Skellefteå, Sweden temperature is an important meteorological parameter because of amount of district heating customers. The MERRA dataset covers the whole earth and the data are compared with ground measurements in Skellefteå. Figure 27 shows the MERRA dataset referenced to the meteorological station at the airport of Skellefteå (64.6°N, 21.1°E). The analysis considers the years of 2012 to 2014. The MERRA data at Skellefteå have a higher negative bias of more than -0.76 K and a RMSE of almost 3 K.

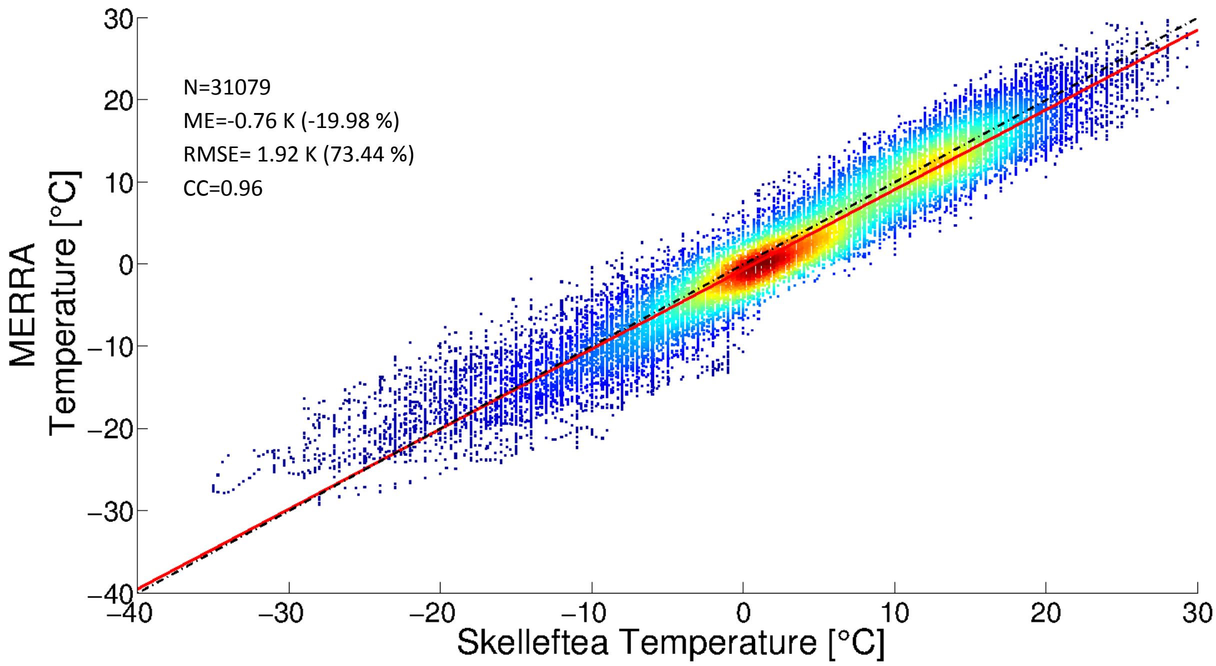

Figure 27: Scatter plot for comparison of MERRA re-analysis data versus a ground measurement at Skellefteå airport weather station. The frequency of occurrence is colour-coded: blue low frequency, red high frequency.

Having ground measurements available, the adjustments from the MERRA data to the local conditions at the measurement site can be done based on such a bias monitoring scheme. Nevertheless, it has to be noted that each consumer/prosumer site will be affected by different effects which cannot be fully and representatively described by the measurements on several sparse location as HS Ulm or Skellefteå. This is a general drawback in using data like MERRA. On the other hand, such re-analysis projects provide a long-term record of analysis fields.

4.2.3 Validation of ECMWF-temperature values with ground measurements

The air temperature is also an important input parameter for the simulation of hybrid grids and the forecast of demand patterns and P_{PV}. While in chapter 4.2.1 and 4.2.2 actual values for the air temperature are used, this chapter investigates air temperature forecasts. The air temperature data are provided by ECMWF. The forecast are calculated as intraday forecast and have a time resolution of 3 hours. The ECMWF data are linearly interpolated to achieve hourly values for the comparison with the DWD weather station. The comparisons between the measured and forecasted data are based on the ME, RMSE and CC (see section 3.1).

The air temperature values of the ECMWF are in UTC time format. The air temperature values from the DWD weather stations are in true solar time so they were linearly interpolated to transfer it into the UTC time format.

In the case of Ulm, the focus is on the calculation of P_{PV}. Therefore, the time between sunrise and sunset is important. For Skellefteå, the focus is the demand in the heat distribution network; hence the accuracy of the air temperature over the whole day is important.

Figure 28 shows the ME values of the comparison between forecasted values with measurements at 35 DWD stations. While for left image all temperature data were considered, the right image shows the ME values comparing measured and forecasted values only of the daylight hours (sun elevation angle >0°). The most values are in the range of -1.5 K to 1.5 K. A positive ME shows that in the average the calculated air temperature is higher than the measured one, while a negative ME reflects lower air temperature forecast values. The range of the ME is very low and it is assumed that the prediction is usable for the calculation of the heat demand in Germany. The analysis for measured values in Skellefteå is in progress. As expected, there is a correlation between the altitude of the ground station and the ME [63]. All the error values, higher than 3 K or lower than -3 K, are registered at locations with an altitude higher than 700 m.

There are differences depending if the night time is considered or not. Without nighttime the forecast underestimates the air temperature for the most locations. Only location 7, 34 and 35, all higher than 870 m, are significant overestimated in the forecast. In regard to the P_{PV} calculation this underestimation can lead to an overestimation in production. In case of the heat demand calculation the demand will be overestimated.

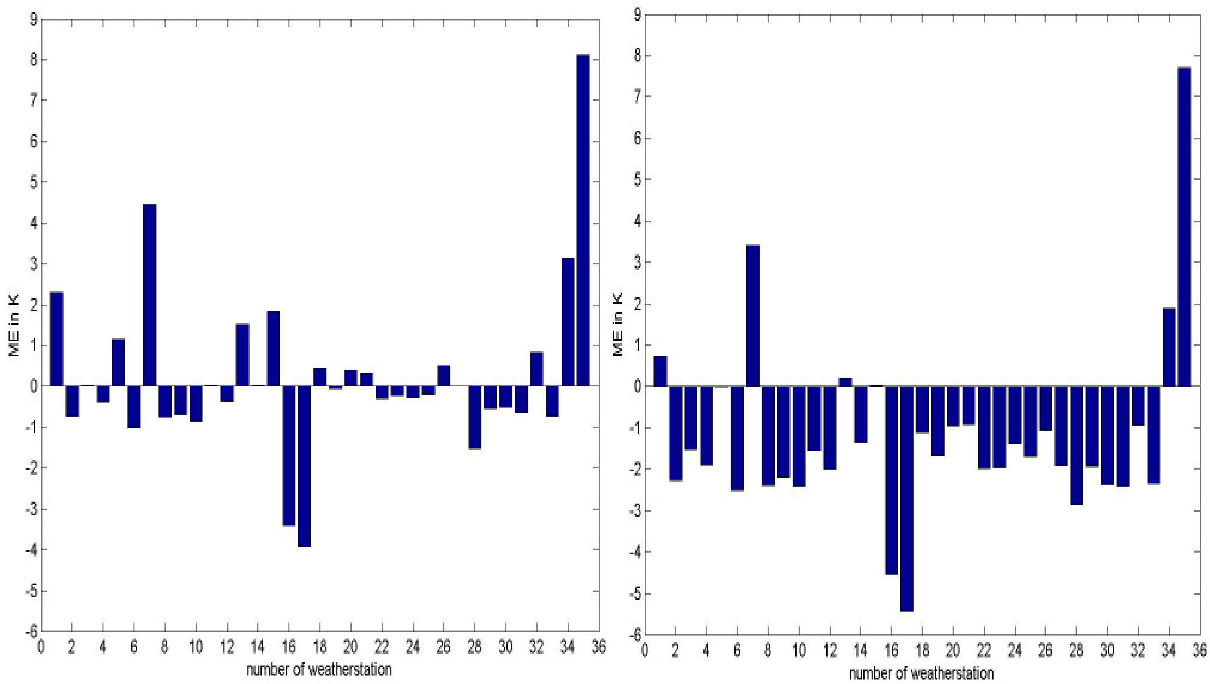

Figure 28: ME of the air temperature of ECMWF intraday forecast and ground measurement at the DWD weather stations. Left image including night time, right image only for sun elevation angles above 0°.

The RMSE values for the comparison between measured and forecast data including the nighttime are shown in Figure 29. The range of the RMSE values is from 6 K to 11 K. The RMSE values show the high variability in the air temperature prediction. The effects of these results have to be evaluated for the application in the heat demand calculation and P_{PV} calculation. The RMSE values the “daytime only” comparisons are similar and a constant variability can be assumed for both periods with and without the night.

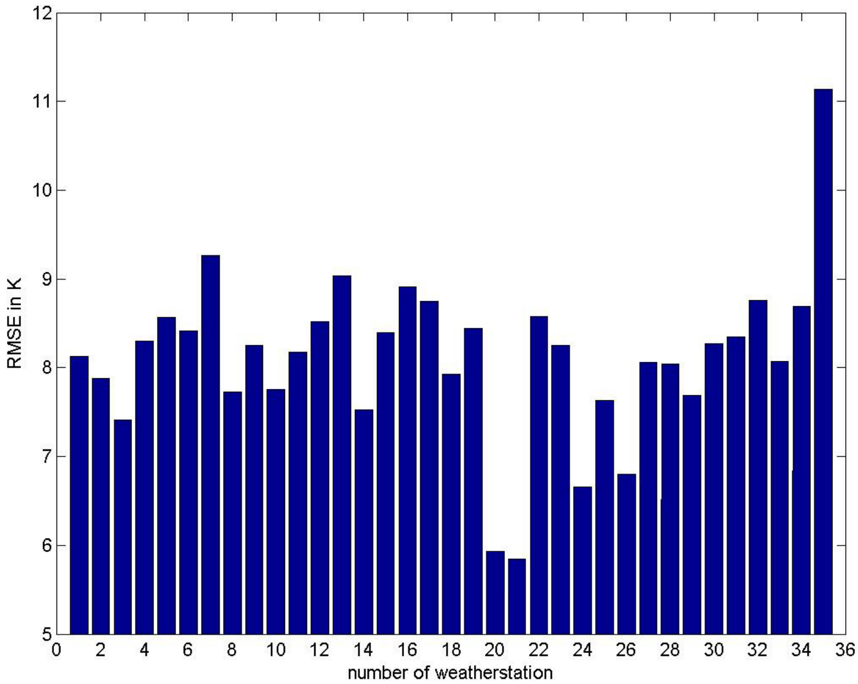

Figure 29: RMSE values for the comparison between measured and forecast data included the nighttime

The CC values for the comparison between measured and forecasted air temperature data including the nighttime are shown in Figure 30: CC values for the comparison between measured and forecast temperature included the nighttime. The CC ranges from 0.45 to 0.625 while the range of the CC for "only daytime" is similar but slightly wider from 0.44 to 0.65. The correlation decline compared with ground measurements or the MERRA reanalysis data but provides the opportunity for upcoming events. This opportunity is a benefit in the operation of the grids or market-oriented decisions for the generator operation times.

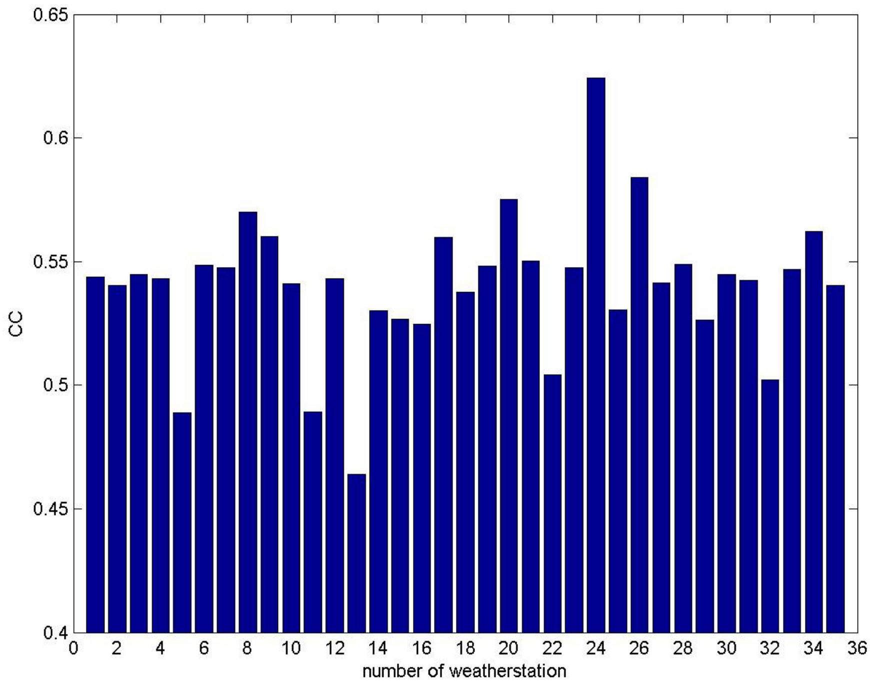

Figure 30: CC values for the comparison between measured and forecast temperature included the nighttime

5 Conclusions and outlook

The results explained in this deliverable show the opportunity and usability of a combination of remotely sensed and in-situ measured observations. The direct comparison shows higher error ranges for the remote sensing data which nevertheless have the advantage of no installation needed at specific locations. This reduces the amount of communications of decentralized devices. The application of the remotely-sensed irradiance measurement in electric low voltage grid of the test site of Ulm shows also further impact factors as the unknown load consumption. This issue needs further investigations and research in future. Furthermore, weather forecasts are foreseen to be implemented into the identical calculation scheme.

The results of the analyses above are the definition of several metrics for the use of remotely sensed information which shall be measured for the optimization of hybrid energy grids and used as an alternative to costly in-situ measurements. These values are the solar irradiance, air temperature, and production and demand inside the electric low voltage grid. The air temperature is an important indicator for heat consumption related to district heating grids and gas grids (Skellefteå and Ulm) while the solar irradiance and electric low voltage grid parameters are important for distributed PV systems and the electric grid (Ulm).

For both metrics ground measurements provide the highest accuracy but also a limited spatial information. The validations show that both meteorological metrics are also accessible by remote sensing measurements. The solar irradiance can be measured using satellite data providing information over large areas. The advantages are long measurement history also for locations without ground measurements because of the long availability of satellite measurements and the near real-time access. The disadvantages are higher errors for a given location.

The study at the test site Einsingen shows the ability of feed-in power determination using remotely sensed irradiance data for PV systems in a small-scale low voltage distribution grid. The combination of this calculation scheme with load profile data from the connected households allows the estimation of the load flow at the transformer station. Both the PV feed-in power and the load flow at the transformer is validated against accurate measurements. One outcome is the strong effects of the load profile used to the statistical results especially during the morning and evening hours. Coupled by the give grid impedance the voltage drop is also affected by the load flow and therefore by clouds reducing the solar irradiance if PV systems are connected to the grid. This correlation is shown in the comparison of cloud data by satellites and in-situ voltage measurements at the transformer.

However, the application of satellite-derived irradiance data in electric grid system calculation with a high number of PV systems shows that the errors of using “virtual measurements” are in the same range or lower as the assumed state-of-the-art load profiles.

The air temperature can be measured directly at the location of interest, also long-term history data can be provided by reanalysis data e.g. MERRA. The comparison with ground stations shows good statistical measures. Therefore the temperature reanalysis data are helpful in planning hybrid grid and gives a required ambient parameter for the simulation of control strategies for hybrid grids.

The air temperature also affects the assets of the grid as shown in the extension of the transformer aging approach. The real air temperatures are used in combination with a transformer housing model to extend the calculation according to [50]. However, the validation is missing but in preparation.

Furthermore, the accuracy of air temperature forecasts for given locations are investigated for the ECMWF data. For intraday forecast the considering the whole day lead to a higher bias compared with the air temperature only when the sun is above the horizons. The variability is similar in both cases. The error ranges have to be considered in the development of applications for the hybrid grids depending on the specific issue.

Recommended measurement points in the electric distribution grid are the distributed generators (e.g. PV, CHP) and physical coupling points to other energy grids. Furthermore, the substations to the medium voltage grid are also recommended for measurements. Depending on the national building standards and typical heating systems the air temperature is an important factor for the demand calculation in all energy forms.

The defined metrics and the validation results of the remote sensing techniques for the solar irradiance and air temperature will be delivered to WP4 and WP5. Beside the ground measurements the data from satellite are used to fill gaps in the measurements or to provide additional information. These data are adapted and applied in the testing phase for different demonstration scenarios.

Moreover, inverters of DES and smart meters offer a further way to monitor the electric grid at the connection points and ensure a secured way for the data transfer. But thereby the challenge is the connection of the different existing measurement systems to the grid control system. Especially, the data transfer has to respect the different privacy issues of the stakeholders. An example for an approach to use existing data for supporting grid operators is the PV inverters. These inverters measure the different grid parameters e.g. voltage, frequency, load flow and power factor at the connection point. The accuracy of the inverter-integrated voltage measurements is in a range of

0.5 % to 2 %. These values are necessary for a control and operation scheme according to national and international standards.

It is assumed that the combination of both, in-situ measurements in near real-time and forecasts based on models will support combined strategies for hybrid grids.

6 Bibliography

[1] European Comission:"Benchmarking smart metering deployment in the EU-27 with a focus on electricity", Brussels 2014

[2] Joint Research Center: http://ses.jrc.ec.europa.eu/smart-metering-deployment-european-union

[3] A. Abdel-Majeed and M. Braun, “Low voltage system state estimation using smart meters,” in Universities Power Engineering Conference (UPEC), 2012 47th International, 2012, pp. 1–6.

[4] T. Kaufman, G. Heilscher, C. Kondzialka, S. Hess, R. Müller, T. Girbig, H. Ruf, M. Casel, M. Gerdes, F. Meier, M. Gmehlin, J. Benken, J. Littwin: “Stand der Technik: Einspeisemanagement mit dem Smart Meter Gateway“, in Proceedings of the 30. Symposium Photovoltaische Solarenergie, Kloster Banz, Bad Staffelstein, Regensburg, 2015.

[5] A. Drews, A. C. Keizer, H. G. Beyer, E. Lorenz, J. Betcke, W. G. J. H. M. van Sark, et al. (2007), “Monitoring and remote failure detection of grid-connected PV systems based on satellite observations” In Solar Energy 81 (4), pp. 548–564.

[6] C. A. Gueymard, “Direct and indirect uncertainties in the prediction of tilted irradiance for solar engineering applications,” Solar Energy, vol. 83, no. 3, pp. 432–444, http://www.sciencedirect.com/science/article/pii/S0038092X08002983, 2009.

[7] D. Renné, “Emerging Meteorological Requirements to Support High Penetrations of Variable Renewable Energy Sources: Solar Energy,” in *Weather matters for energy*, A. Troccoli, L. Dubus, and S. E. Haupt, Eds, 2014, pp. 257–273.

[8] H. Ruf, M. Schroedter-Homscheidt, F. Meier, G. Heilscher: "Using satellite data for power flow estimation of an electrical low voltage grid with a high amount of photovoltaic systems", at International Conference Energy & Meteorology, Boulder, Colorado ,June 2015, http://icem2015.org/wp-content/uploads/2015/07/1350_HolgerRuf.pdf

[9] K. Ogimoto, K. Washihara, I. MacGill, B. Mather, T. Stetz, C. Mayr, R. Bründlinger, A. Iaria, E. Gaglioti, M. Rekinger, K. de Brabandere, S. Tselepis, J. Remund, C. Bucher, K. Frederiksen, Y. Wang, B. Kulwaree: ”High Penetration PV in Power Systems Outcome of the IEA-PVPS Task 14’s Subtask 3”, 29th EUPVSEC Amsterdam 22 - 26 Sept 2014, Amsterdam, Netherlands; 09/2014

[10] D. Heinemann, E. Lorenz, K. Pagh Nilsen,J. Remund, S.c. Müller, W. Traunmüller: "Comparison of Irradiance Forecasts based on Numerical Weather Prediction for Central and Northern Europe”, at International Conference Energy & Meteorology, Boulder, Colorado ,June 2015, http://icem2015.org/wp-content/uploads/2015/07/1150_DetlevHeinemann.pdf

[11] Project EWeLiNE: http://www.projekt-eweline.de/

[12] www.bsrn.awi.de

[13] www.dwd.de

[14] D. Cano, J. Monget, M. Albuisson, H. Guillard, N. Regas, and L. Wald, “A method for the determination of the global solar radiation from meteorological satellite data,” Solar Energy, vol. 37, no. 1, pp. 31–39, 1986.

[15] H. G. Beyer, C. Costanzo, and D. Heinemann, “Modifications of the Heliosat procedure for irradiance estimates from satellite images,” Solar Energy, vol. 56, no. 3, pp. 207–212, 1996.

[16] A. Hammer, D. Heinemann, C. Hoyer, R. Kuhlemann, E. Lorenz, R. Müller, H.G. Beyer, “Solar energy assessment using remote sensing technologies”, Remote Sensing of Environment 86 (3), pp. 423–432.

[17] G. Heilscher, M. Gmehlin, J. Conrad, and A. Ehm, “Concept for Large-Scale-Deployment of Grid Connected PV in the Private Sector at the Edge of Grid Parity,” in 25th World Conference on Photovoltaic Energy Conversion: Proceedings, Valencia, Spain, 2010, pp. 5305–5308.

[18] H. G. Beyer, J. P. Martinez, M. Suri, J. L. Torres, E. Lorenz, S. Müller, C. Hoyer-Klick, and P. Ineichen, “Report on Benchmarking of Radiation Products: Deliverable 1.1.3,” Aug. 2009. [Online]. Available: www.mesor.org/docs/MESoR_Benchmarking_of_ radiation_products.pdf

[19] M. Lefèvre, A. Oumbe, P. Blanc, B. Espinar, B. Gschwind, Z. Qu, L. Wald, M. Schroedter-Homscheidt, C. Hoyer-Klick, A. Arola, A. Benedetti, J. W. Kaiser, and J.-J. Morcrette, “McClear: a new model estimating downwelling solar radiation at ground level in clear-sky conditions,” Atmospheric Measurement Techniques, vol. 6, no. 9, pp. 2403–2418, [Online]. Available: www.atmos-meas-tech.net/6/2403/2013/, 2013.

[20] A. Oumbe, Z. Qu, P. Blanc, M. Lefèvre, L. Wald, and S. Cros, “Decoupling the effects of clear atmosphere and clouds to simplify calculations of the broadband solar irradiance at ground level,” Geoscientific Model Development Discussions, vol. 7, no. 2, pp. 2007–2032, 2014.

[21] B. Espinar, C. Hoyer-Klick, M. Lefevre, M. Schroedter-Homscheidt, and L. Wald, “USER’S GUIDE to the MACC-RAD Services on solar energy radiation resources: v3 - July 2014 - MACC-II Deliverable 122.6,” Project MACC-II, Armines, Jul. 2014.

[22] DLR, Hourly global and direct normal irradiance for Europe, Africa and Asia. Available: https://wdc.dlr.de/data_products/SERVICES/SOLARENERGY/description.php (2015, Apr. 25).

[23] Z. Qu, A. Oumbe, P. Blanc, M. Lefevre, L. Wald, M. Schroedter-Homscheidt, G. Gesell, and L. Klueser, “Assessment of Heliosat-4 surface solar irradiance derived on the basis of SEVIRI-APOLLO cloud products,” in Proceedings of the 2012 EUMETSAT Meteorological Satellite Conference, Sopot, Poland, 2012.

[24] H. G. Beyer, J. Betcke, A. Drews, D. Heinemann, E. Lorenz, G. Heilscher, and S. Bofinger, “Identification of a general model for the MPP performance of PV-modules for the application in a procedure for the performance check of grid connected systems,” in Nineteenth European Photovoltaic Solar Energy Conference: Proceedings of the international

conference held in Paris, France, 7-11 June 2004, München, Florence: WIP-Renewable Energies; ETA, 2004, pp. 3073–3076.

[25] J. S. Stein, "The photovoltaic Performance Modeling Collaborative (PVPMC)," in Photovoltaic Specialists Conference (PVSC), 2012 38th IEEE: Date, 3-8 June 2012, Piscataway, NJ: IEEE, 2012, pp. 003048–003052.

[26] https://www.gmes-atmosphere.eu/

[27] C. Hoyer-Klick, M. Lefèvre, M. Schroedter-Homscheidt, L. Wald, "USER'S GUIDE to the MACC-RAD Services on solar energy radiation resources March2015," MACC III D57.5

[28] A. Zelenka, R. Perez, R. Seals, and D. Renné, "Effective Accuracy of Satellite-Derived Hourly Irradiances," Theoretical and Applied Climatology, vol. 62, no. 3-4, pp. 199–207, 1999.

[29] Weather data from DWD, Ulm, checked 20.04.2015 http://www.dwd.de/bvbw/generator/DWDWWW/Content/Luftfahrt/Internetservice/stations__10,templateId=raw,property=publicationFile.pdf/stations_10.pdf

[30] Solar Radiation Data Service
www.SoDa-pro.com

[31] D. Reindl, W. Beckman, and J. Duffie, "Diffuse fraction correlations," Solar Energy, vol. 45, no. 1, pp. 1–7, 1990.

[32] D. Reindl, W. Beckman, and J. Duffie, "Evaluation of hourly tilted surface radiation models," Solar Energy, vol. 45, no. 1, pp. 9–17, 1990.

[33] H. Ruf, D. Funk, F. Meier, and G. Heilscher, "Bestimmung von Ausrichtungs- und Neigungswinkeln von Bestandsanlagen mittels LIDAR Daten," in Proceedings of the 30. Symposium Photovoltaische Solarenergie, Kloster Banz, Bad Staffelstein, Regensburg, 2015.

[34] P. Loutzenhiser, H. Manz, C. Felsmann, P. Strachan, T. Frank, and G. Maxwell, "Empirical validation of models to compute solar irradiance on inclined surfaces for building energy simulation," Solar Energy, vol. 81, no. 2, pp. 254–267.

[35] D. L. King, W. E. Boyson, and J. A. Kratochvill, "Photovoltaic Array Performance Model," Sandia National Laboratories, Albuquerque, Sandia Report SAND2004-3535, 2004.

[36] D. L. King, S. Gonzalez, G. M. Galbraith, and W. E. Boyson, "Performance Model for Grid-Connected Photovoltaic Inverters," Sandia National Laboratories, Albuquerque, Sep. 2007.

[37] S. W. Glunz, R. Preu, and D. Biro, "Crystalline Silicon Solar Cells," in Comprehensive Renewable Energy, A Sayigh, Ed.: Elsevier, 2012, pp. 353–387.

[38] G. Wirth, A. Spring, G. Becker, R. Pardatscher, M. Lödl, R. Witzmann, J. Brantl, M. Garhamer, and H. Wagenhäuser, "Felduntersuchung der Netzauslastung und Spannungsanhebung durch PV-Anlagen," in Proceedings of the 26. Symposium Photovoltaische Solarenergie, Kloster Banz, Bad Staffelstein, Regensburg, 2011.

[39] C. Rigollier, M. Lefèvre, and L. Wald, “The method Heliosat-2 for deriving shortwave solar radiation from satellite images,” Solar Energy, vol. 77, no. 2, pp. 159–169, 2004.

[40] L. F. Zarzalejo, J. Polo, L. Martín, L. Ramírez, and B. Espinar, “A new statistical approach for deriving global solar radiation from satellite images,” Solar Energy, vol. 83, no. 4, pp. 480–484, 2009.

[41] R. Mueller, K. Dagestad, P. Ineichen, M. Schroedter-Homscheidt, S. Cros, D. Dumortier, J. Olseth, G. Piernavieja, C. Reise, L. Wald, and D. Heinemann, “Rethinking satellite-based solar irradiance modeling - The SOLIS clear-sky module,” Remote Sensing of Environment, vol. 91, no. 2, pp. 160–174, 2004.

[42] S. Krauter, P. Grunow, A. Preiss, S. Rindert, and N. Ferretti, “Inaccuracies of input data relevant for PV yield prediction,” in 2008 33rd IEEE Photovolatic Specialists Conference (PVSC), pp. 1–5.

[43] K. Behrens, R.-D. Grewe, “A Comparison of SCAPP radiation data with global, diffuse and direct solar radiation,” in: Technical Conference on Meteorological and Environmental Instruments and Methods of Observation <Bucharest, Romania, 2005>: Papers presented at the WMO Technical Conference on Meteorological and Environmental Instruments and Methods ob Observation (TECO-2005) ; Session 1 (Papers),8 ; S. 1 - 7

[43] H. Ruf, D. Stetter, S. Lanig, C. Hoyer-Klick, F. Meier, G. Heilscher, “Active Grid Planning Based on Solar Power Roof Potential Analysis”. in 27th European Photovoltaic Solar Energy Conference. Proceedings of the International Conference held in Frankfurt a. M, 24-28 September 2012. München: WIP, pp. 3782–3787.

[45] R. R. Perez, P. Ineichen, R. D. Seal, E. L. Maxwell, and A. Zalenka, “Dynamic global-to-direct irradiance conversion models,” (eng), ASHRAE Transactions, vol. 98, no. 1, pp. 354–369, http://archive-ouverte.unige.ch/unige:38583, 1992.

[46] www.bdew.de

[47] K. Engels, Probabilistische Bewertung der Spannungsqualitat in Verteilungsnetzen, 1st ed. Aachen: Klinkenberg Verlag, 2000.

[48] www.ulm-netze.de

[49] Siemens; Prüflabor für Transformatoren Materialien; Lebensdauer; checked 12.09.2014 http://www.energy.siemens.com/hq/de/services/stromuebertragung/transformatoren-prueflabor/#content=Lebensdauer

[50] DIN 60076- Power transformers - Part 7: Loading guide for oil-immersed power transformers
a) S.30, 8.3.2 Korrektur der Umgebungstemperatur für das Transformatorgehäuse

[51] Betonbau, technical data manual compact station UK 3015, von 09/2008, checked 16.12.2014

[52] Recknagel, Sprenger Schramek, Heizung + Klima Technik 03/04, 2003

[53] Deutscher Wetterdienst, CDC - Climate Data Center, checked 17.4.2015

[54] ASHRAE Handbook, Atlanta, GA: American Society of Heating, Refrigerating and Air Conditioning Engineer, 2009

[55] Andreas Küchler, Hochspannungstechnik, Grundlagen - Technologie- Anwendungen; 3., neu bearbeitete und erweiterte Auflage; Springer-Verlag

[56] K. T. Kriebel, G. Gesell, M. Kästner, and H. Mannstein, “The cloud analysis tool APOLLO: Improvements and validations,” International Journal of Remote Sensing, vol. 24, no. 12, pp. 2389–2408, 2003.

[57] H. Ruf, M. Schroedter-Homscheidt, H. G. Beyer, F. Meier, and G. Heilscher, “Analysis of Cloud Indicators to Derive the Bus Bar Voltage at a Local Low Voltage Distribution Grid Transformer,” in Proceedings: 28th European Photovoltaic Solar Energy Conference and Exhibition : Parc des Expositions Paris Nord Villepinte, Paris, France : conference, 30 Sep-04 Oct 2013, exhibition, 01 Oct-03 Oct 2013, 2013, p. 3944.

[58] www.endorse-fp7.eu

[59] S. Serpico, G. Moser, M. De Martino, “ASSESSMENT OF AIR TEMPERATURE AT 2 m”, Project ENDORSE. D3.3. Univerity of Genoa. Available online at http://www.endorse-fp7.eu/sites/www.endorse-fp7.eu/files/docs/D3.3_rev30apr12.pdf.

[60] M.M. Rienecker, M. Suarez, R. Gelaro, R. Todling, J. Bacmeister, E. Liu, et al. ,“MERRA: NASA’s Modern-Era Retrospective Analysis for Research and Applications“, J. Climate 24 (14), pp. 3624–3648.

[61] S. Krauter, P. Grunow, A. Preiss, S. Rindert, and N. Ferretti, “Inaccuracies of input data relevant for PV yield prediction,” in 2008 33rd IEEE Photovolatic Specialists Conference (PVSC), 2008, pp. 1–5.

[62] N. Gilet, A. Mahura, C. Petersen, B. H. Sass (2013), “Analysis and improvement of statistical error in forecasted air temperature” DMI Scientific Report 13-03. Available online at http://www.dmi.dk/fileadmin/user_upload/Rapporter/SR/2013/sr13-03.pdf

[63] Ch. Ch. Ling:“Einführung in die Meteorologie“, Hochschule für Technik, Zürich,1988

[64] G. Heilscher, H. A. A. Correa, F. Ebe, T. Kaufmann, H. Ruf, R. Müller, F. Meier, „Qualifizierung der Netzspannungsinformation von Wechselrichtern für die Beurteilung des Netzzustands von Niederspannungsnetzen“, 29. Symposium Photovoltaische Solarenergie. 12. bis 14. März 2014,Kloster Banz, Bad Staffelstein. 29. Symposium Photovoltaische Solarenergie. Kloster Banz, Bad Staffelstein, 12. bis 14. März 2014. OTTI. 1 volume. 1st ed. Regensburg.

[65] T. Kaufmann, G. Heilscher, S. Hess, R. Müller, M. Gerdes, F. Meier, M. Gmehlin, „Einspeisemanagement mit dem Smart Meter Gateway“, 29. Symposium Photovoltaische Solarenergie. 12. bis 14. März 2014,Kloster Banz, Bad Staffelstein. 29. Symposium Photovoltaische Solarenergie. Kloster Banz, Bad Staffelstein, 12. bis 14. März 2014. OTTI. 1 volume. 1st ed. Regensburg.

[66] C. Reese, M. Mohrmann, L. Hofmann, M. John, „Umsetzung eines Verfahrens zum Einsatz von Ortsnetztransformatoren als Messwandler im Netzbetrieb“, VDE Kongress 2012 Smart Grid: Intelligente Energieversorgung der Zukunft, Proceedings 5. - 6. November 2012, Internationales Congresscenter Stuttgart (ICS): VDE VERLAG.

[67] C. Matrose, M. Gödde, M. Cramer, F. Potratz, T. Pollok, A. Schnettler, „Anlagenauswahl und –positionierung zur Spannungsstützung mittels Blindleistungsmanagement dezentraler Erzeugungsanlagen“, VDE Kongress 2012 Smart Grid: Intelligente Energieversorgung der Zukunft, Proceedings 5. - 6. November 2012, Internationales Congresscenter Stuttgart (ICS), vol. 1: VDE VERLAG.

7 Disclaimer

The OrPHEuS project is co-funded by the European Commission under the 7th Framework Programme “Smart Cities” 2013.

The sole responsibility for the content of this publication lies with the authors. It does not necessarily reflect the opinion of the European Commission.

The European Commission is not responsible for any use that may be made of the information contained therein.

8 Contacts

Project coordinator

Ingrid Weiss & Silvia Caneva @ WIP – Renewable Energies

Sylvensteinstrasse 2, Munich, Germany

Email: Ingrid.weiss@wip-munich.de / Telephone: 0049 (0) 720 12 742

Email: silvia.caneva@wip-munich.de / Telephone: 0049 (0) 720 12 733

WP Leader

Holger Ruf @ Ulm University of Applied Science

Institute for Energy and Drive Technologies
Eberhard Finckh Str. 11
D-89075 Ulm

Phone: +49(0)731 50 28348

Email: ruf@hs-ulm.de